ISSN 1063-7796, Physics of Particles and Nuclei, 2019, Vol. 50, No. 1, pp. 42–76. © Pleiades Publishing, Ltd., 2019.
Russian Text © Yu.N. Kharzheev, 2019, published in Fizika Elementarnykh Chastits i Atomnogo Yadra, 2019, Vol. 50, No. 1.

Radiation Hardness of Scintillation Detectors Based on Organic Plastic Scintillators and Optical Fibers

Yu. N. Kharzheev*

Dzhelepov Laboratory of Nuclear Problems, Joint Institute for Nuclear Research, Dubna, Russia

**e-mail: kharzheev@mail.ru*

Abstract—Scintillation detectors (SD) based on organic plastic scintillators and optical fibers are basic detectors at all modern accelerators and in astrophysics and neutrino physics experiments. In recent years, interest in SD has significantly increased due to the upcoming major upgrade of the LHC and the construction of new accelerators NICA, FAIR, FCC, etc. At the same time, requirements on the stability and reliability of SD operation under new conditions have become stricter, and their fulfillment largely depends on radiation hardness of scintillators, optical fibers, and photodetectors. The review presents the results of the radiation hardness investigations of various scintillators, optical fibers (scintillating, as well as wavelength-shifting and clear), and optical glues used to increase light collection from scintillators by fibers. The influence of various factors (dose, dose rate, type of radiation, scintillator materials, and fluors) on light output, light collection, and transmittance of the irradiated materials and their recovery is considered. Aging of scintillators caused by environmental effects (temperature, humidity) irrespective of radiation is also briefly considered.

DOI: 10.1134/S1063779619010027

CONTENTS

INTRODUCTION

Scintillation detectors based on organic plastic scintillators and optical fibers have been efficiently and reliably employed in many high-energy physics (HEP) experiments for many decades [1, 2]. They are basic detectors in all modern accelerator, astrophysics, and neutrino physics experiments due to their time-stable optical and spatio-temporal characteristics, high detection efficiency for charged particles, ease of manufacture and use, and low cost [3]. In the past years, interest in SD has greatly increased in view of the upcoming major upgrade of the LHC [4] and construction of new accelerators FCC [5], FAIR [6], NICA [7], etc.

The scintillators most commonly used in SD are polystyrene (PS) and polyvinyl toluene (PVT). However, their light yield is low due to the self-absorption of intrinsic radiation. Therefore, the scintillators used in experiments are usually three-component mixtures of a PS or PVT base with a small amount of fluors, primary (activators) and secondary (wavelength shifters), dissolved in it.

Light collected from the scintillators is transported to the photodetector (PD) by wavelength-shifting (WLS) fibers inserted in special grooves on the surface of tiles or in the through holes of strips. Fibers are often glued into the grooves to improve their optical contact with the scintillator and increase light collection, and optically clear fibers (CF) are often used to

increase the efficiency of light transport from the WLS fibers to a distant PD.

Scintillating fibers (SciFi) are widely used in HEP experiments, usually in very high radiation areas, for measurement of beam luminosity, determination of particle coordinates, time-of-flight separation of particles, triggering, etc.

Scintillation detectors for modern and future experiments consist of many small tiles (in calorimeters) and long narrow strips (in neutrino and other detectors). Photodetectors to be used with these SD must meet a range of strict requirements on quantum efficiency, light collection homogeneity, pixelation, compactness, energy efficiency (cost), size, and sensitivity to the magnetic field. All these requirements are largely met by silicon photodetectors (SiPMs), and therefore they oust traditional photomultiplier tubes. However, they have some drawbacks to be taken into account, such as high sensitivity to temperature variation (dark currents) and low radiation hardness as compared to photomultiplier tubes.[1]

Scintillators, optical fibers, and PD used at modern accelerators are subject to high radiation loads, which results in deterioration (damage) of light yield and transmittance of both the scintillator base and the fluors, deterioration of light collection and transport by WLS fibers, changes in their mechanical properties, and damage of the PD structure. Therefore, scintillators and optical fibers are tested for radiation hardness before being put into service.

Upgrading activities at the ATLAS [9], CMS [10], LHCb [11], and other spectrometers involve investigations of both known and new scintillator and fiber materials capable of meeting the increasingly strict radiation hardness requirements.

The issues considered in this review are radiation hardness studies of various scintillators and optical fibers and the level of their damage in relation to the absorbed dose, dose rate, type of irradiating particles, and fluor and scintillator materials and recovery of irradiated scintillators and fibers.

Abbreviations used in the text

PS $(C_8H_8)_n$, PVT $(C_9H_{10})_n$, polystyrene and polyvinyl toluene respectively, the main materials used as a scintillator base.

PPMA $(C_5O_2H_8)_n$, polymethyl methacrylate, often used for the inner cladding of multiclad fibers.

PPO ($C_{15}H_{11}NO$), 2,5-diphenyloxazole.

pTP ($C_{18}H_{14}$), *para*-terphenyl.

POPOP ($C_{24}H_{16}N_2O$),1,4-di-(5-phenyl-2-oxazolyl)-benzene.

3HF (3-hydroxyflavone), Y11, Y(8), K27, wavelength shifters.

WLS, SciFi, and CF, wavelength-shifting, scintillating, and clear fibers.

S type/non-S type WLS fibers, fibers with oriented/uniformly distributed molecules.

PD, photodetector

1. RADIATION LOAD AT EXISTING AND PROJECTED ACCELERATORS

Many detectors used at modern accelerators are located in areas with a very high radiation load. Among these detectors based on organic scintillators and optical fibers are electromagnetic and hadronic calorimeters and tracking and time-of-flight detectors.

The radiation pattern in a one-quarter of the ATLAS spectrometer at the LHC at luminosity of about 10^{34} cm^{-2} s^{-1} is shown in Fig. 1 [8]. Ten years of the LHC operation can bring the radiation load to 10 Mrad for the hadronic calorimeter of the CMS HE spectrometer [9] and to 3.5 Mrad for the scintillating fiber tracking detector of the LHCb spectrometer near the beam pipe [10].

At the projected accelerators, luminosity may substantially increase, e.g., to 5×10^{34} cm^{-2} s^{-1} at the High Luminosity LHC (HL-LHC) (by 2025), and at NICA [7] it can be 10^{27} cm^{-2} s^{-1} of Au^{79+} ions (see Table 1). In addition to charged particles, a large number of neutrons are produced in hadronic and electromagnetic showers in calorimeters and in other areas in accelerators, which may cause considerable radiation damage. For example, the neutron flux at the LHC can reach the level of over 10^{15} cm^{-2} in one year [4], and high neutron fluxes can also be expected far from the beam pipe, e.g., in the CRV–TS module (part of the cosmic muon veto system) of the Mu2e spectrometer (Fig. 1b): 10^{11} cm^{-2} in its working period [11].

2. SCINTILLATION LIGHT GENERATION IN ORGANIC SCINTILLATORS, THEIR RADIATION DAMAGE AND RECOVERY

Passing through a scintillator, an ionizing particle loses its energy to excite and ionize scintillator molecules, which results in transfer of π electrons to higher energy states, the transition from which to the ground state is through the singlet S_1 or, rarely, triplet T_1 states. The transition is accompanied by emission of fast scintillation photons (10^{-9}–10^{-8} s) (fluorescence) in the former case and slow photons (10^{-4} s) (phosphorescence) in the latter.

However, the most often used PS- and PVT-based scintillators feature high self-absorption of intrinsic radiation, and therefore three-component scintillators are normally preferred. The scintillator base is doped with a small amount of fluors, 1–2% of activators (PPO, PTP, PBD) and 0.01–0.04% of wavelength

[1] PD will not be considered in this review.

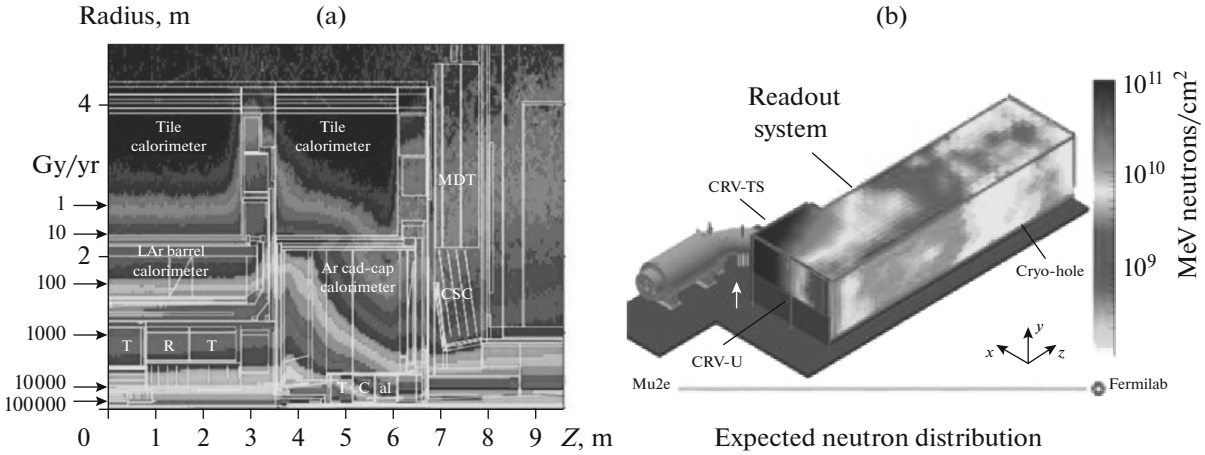

Fig. 1. Radiation pattern at the LHC ATLAS spectrometer [4] (a) and Mu2e CRV module [11] (b).

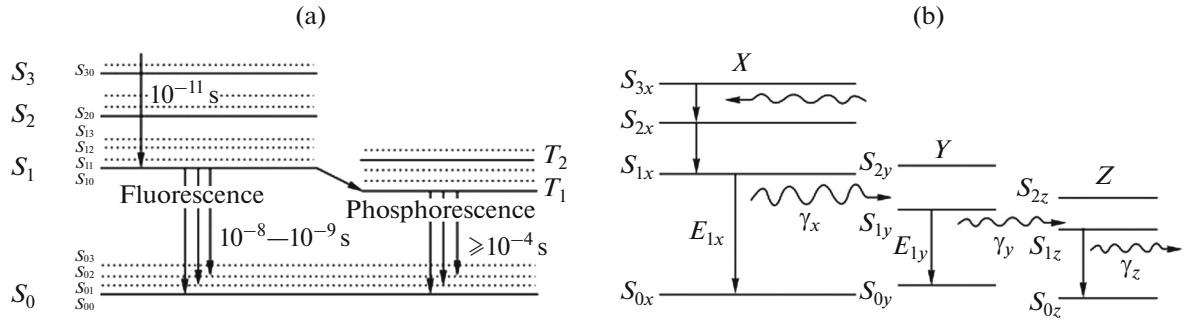

Fig. 2. Scheme of scintillation light generation in a one-component (a) and a three-component scintillator (b) [13].

shifters (POPOP). Energy of excited base molecules is radiationlessly transferred via dipole-dipole interaction to activator molecules (Förster mechanism [12]). Excited activator molecules return to the ground state with emission of photons in the wavelength region of about 370 nm, which is in the absorption region of wavelength shifters. The scheme of scintillation light generation in a one-component and a three-component scintillator is shown in Figs. 2a and 2b [13].

Wavelength shifters absorb these photons and reemit them with wavelengths close to the spectrum sensitivity of the most commonly used PDs. The fluors are selected with allowance for shifts in radiation spectra and absorption of the corresponding components (Stokes shift). Table 2 presents positions of the peaks of the absorption and emission spectra and their difference for a number of popular fluors.

Scintillation light from the scintillator base is collected, reradiated, and transported to the PD through WLS fibers, which have almost ousted the cumbersome acrylic light guides.

PS $(C_8H_8)_n$ and PVT $(C_9H_{10})_n$ are aromatic hydrocarbon polymers consisting of benzene rings bonded to the methyl (CH_3–) and vinyl (CH_2–CH–) groups respectively (Figs. 3a, 3b). Scintillators are sometimes

Table 1. Luminosities at existing and projected accelerators

Accelerator	Luminosity	Particles	Energy	Ref.
LHC, HL-LHC	2×10^{34} cm^{-2} s^{-1} (now) ~5×10^{34} cm^{-2} s^{-1} (by 2025)	P + P	14 TeV 14 TeV	4
FCC	5×10^{34} cm^{-2} s^{-1} (2035)	P + P	100 TeV	5
FAIR (HESR)	10^{32} cm^{-2} s^{-1} (2025)	antiP + ions	1–16 GeV	6
NICA	10^{27} cm^{-2} s^{-1} (2020)	Au^{79+} ions	4–11 GeV	7

Table 2. Characteristics of some popular fluors [14]

Fluor	Peak absorption length, nm	Peak emission length, nm	Difference between peak absorption and emission lengths, nm
PBD	305	365	60
b-PBD	310	365	55
BDB	360	405/425	45/65
Y7	437/460	490	63/30
3HF	350	530	180
m3HF	350	430	80
Y11	430	476	46
POPOP	361	415	54
PPO	310	365	55
K27	355	492	37
pTP	290	360	70
Naphthalene	310	325/340	15/30
X25	400	500	100
X31	400	500	100

made on the basis of PMMA $(C_5O_2H_8)_n$, though it is most often used for inner clads of optical fibers (Fig. 3c).

Affected by radiation, molecular chains in scintillator bases and WLS fibers suffer damage, breaks, and cross-linking. This leads to changes in the structure of the polymers and production of free radicals (color centers) which absorb and scatter scintillation light and evolve various gaseous products (Table 3) [15]. This all impairs light yield, transmittance (light transport), and mechanical properties of scintillators.

Scintillation light loss is most manifested in the region of ultraviolet and blue wavelengths and least manifested in the longwave region. Therefore, wavelength shifters with a large Stokes shift to the longwave region are usually chosen, such as 3HF, Y11, POPOP, etc.

Radicals also play a significant role in recovery of scintillator light yield and transmittance, and their number depends on the scintillator material, absorbed dose, and dose rate. Radicals are predominantly unstable formations, which can decay or interact with one another. At high dose rates, the formation rate of radicals is high, and the total irradiation time is short. Oxidation processes are not supported due to shortage of O_2. At low dose rates, the situation is the opposite. Recovery of irradiated materials strongly depends on the absorbed dose, dose rate, and environment, and a particular role is played by O_2 [18, 19]. It is usually incomplete and stops at a certain residual constant level.

Table 3 presents gaseous products arising from electron and γ irradiation of some polymers [15], and Table 4 presents *g* values that characterize the amounts of radiation damage in PS and PMMA per 100 eV of absorbed energy in 1 mol of the material: the formation of radicals and gases, degradation of molecules, and cross-linking of chains [16]. The dominant pro-

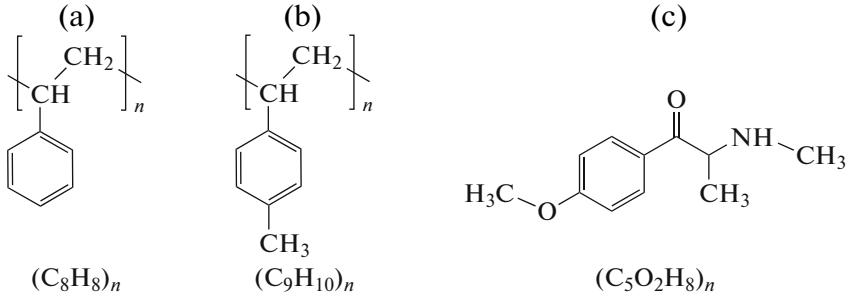

Fig. 3. Structure of the PS-based (a), PVT-based (b), and PMMA-based (c) scintillators.

Table 3. Formation of gaseous products in polymers irradiated with γ rays and electrons at room temperature [15]

Polymer	Product G (molecules per 100 eV)
Polyethylene HD	H_2 ~ 3; CH_4 ~ 0.002
Polypropylene	H_2 ~ 2.5; CH_4 ~ 0.1
Polyisobutylene	H_2 ~1.5; CH_4 ~ 0.5
Polyvinylchloride	HCl ~ 2.7; H_2 ~ 0.15; CH_4 ~ 0.002
Polyvinyl acetate	H_2 ~ 0.6; CH_4 ~ 0.3; CO ~ 0.28; CO_2 ~ 0.06
Polymethyl methacrylate	CH_4 ~ 0.6; CO ~ 0.5; CO_2 ~ 0.4; H_2 ~ 0.2
Polystyrene	H_2 ~ 0.03; $CH_4 \sim 1 \times 10^{-5}$
Poly(alpha-methylstyrene)	H_2 ~ 0.04; CH_4 ~ 0.003

cesses are cross-linking in PS and formation of radicals and degradation in PMMA.

3. RADIATION TESTS OF SCINTILLATORS AND OPTICAL FIBERS AT RADIOACTIVE SOURCES, ACCELERATORS, AND NEUTRON REACTORS

3.1. Scintillators

Fluors. Hadronic calorimeters use scintillating tiles with grooves on their surface for embedding WLS fibers that collect scintillation light, transform its wavelength, and transport it to the PD. In electromagnetic calorimeters of the shashlik type, WLS fibers are laid in special holes running through a stack of alternating layers of scintillating tiles and lead plates. In neutrino experiments, scintillator strips are used with grooves on their surface or with through holes for WLS fibers. Scintillating tiles of various size are used in time-of-flight devices, triggers, and veto systems, in which strips can also be used.

Radiation hardness of scintillators depends not only on their base but also on fluors. Comprehensive radiation hardness investigations of PS- and PVT-based scintillators with different fluors and their concentrations were carried out using ^{60}Co γ rays with a dose of 2.3, 3.3, 10, and 14.3 Mrad [14].

Scintillators with the primary fluors pTP, PPO, PBD, and bPBD showed similar good radiation hardness characteristics, and scintillators with pyrazoline, benzoxazole, BPO, BO, and PBD and ultraviolet scintillators were less radiation hard. PS-based scintillators with secondary fluors, derivatives of naphthalene (X25, X31) in high concentration, and with 3HF and m3HF showed higher radiation resistance.

Radiation hardness of PS-based plastic scintillators was investigated using the ^{60}Co source with a dose of 2.8 Mrad and dose rate of 850 rad/min at different concentrations of fluors, diffusion enhancers, and stabilizers [17].

It was shown that radiation hardness and light yield of scintillators with fluors was higher than those of monomer scintillators, and they slightly increased with increasing concentration of primary fluors. The optimum concentration of pTP is 6%. The increase in the concentration of the most popular secondary fluor (POPOP) causes a slight decrease in the scintillator light yield and transmittance, and its optimum concentration is 0.01–0.02%.

Diffusion enhancers and stabilizers give a considerable gain in light yield and radiation hardness. The scintillator made with 2% pTP + 0.02% POPOP fluors, 20% diffusion enhancer, and 0.01% stabilizer retains 91% of light yield 1.5 h after irradiation.

One of the very radiation-hard fluors is considered to be 3HF, whose absorption spectrum covers emission spectra of popular scintillators and fluors. The effect of radiation on the light yield and transmittance of PS-based scintillators doped only with 3HF and of ternary scintillators, i.e., scintillators with two fluors (1% PTP + 0.1% 3HF and 1% PTP + 0.01% 3HF), was investigated in [18]. Irradiation was performed using ^{60}Co γ rays with the doses of 10 and 30 Mrad depending on the weight concentration (ε) of 3HF

Table 4. Values *g* characterizing amounts of radiation damage in PS and PMMA per 100 eV of absorbed energy in 1 mol of material: formation of radicals R and gases, degradation of molecules, and cross-linking of chains [16]

Process	*g*	
	PMMA	PS
Formation of R	2.4–2.5 [4, 5]	0.2 [6]
Gas formation	1.18 [7] (30.5% CO, 15.7% CO_2, 14.2% $HCOOCH_3$, 13.1% CH_4, 11.7% H_2 ...)	0.026 [7] (100% H_2)
Degradation	[8]	
	1.7–2.6 [9]	0.009 [9]
Cross-linking	0 [9]	0.034 [9]

Table 5. Light yields before (L_0) and after (L) irradiation and their ratios L/L_0 at different doses and postirradiation time periods of several scintillators (borrowed from Tables 1, 3, 4 [14])

Scintillator	L_0,%	L/L_0, % Dose (Mrad)	L/L_0, % Dose (Mrad)	L/L_0, % (Time)
PVT + 2%PBD + 0.01% POPOP	100	72 (3.3)	37 (14.3)	48 (3 mos.)
PS + 2% pTP + 0.025% POPOP	98	71 (2.3)	23 (10)	52 (23 d)
PS + 10%PPO + 0.5% POPOP	98	73 (2.3)	36 (10)	67 (23 d)
PS + 5% N+ 2% pTP + 10% PPO + 0.5% POPOP	71	93 (2.3)	59 (10)	69 (23 d)
PS + 2.0% pTP + 0.025% X25	78	72 (4)	53 (10)	58 (23 d)

ranging from 0.05 to 2.0%. Light yields of nonirradiated and irradiated 3HF scintillators (immediately after irradiation) as a function of ε are shown in Figs. 4 and 5 respectively. In addition, Fig. 4 also shows light yields of pure PS, Bicron 408, and ternary scintillators doped with PTP + 0.01% 3HF and PTP + 0.1% 3HF.

The light yield loss in the 3HF scintillators is seen to increase with decreasing 3HF concentration. At the radiation dose of 10 Mrad the light yield loss of the recovered scintillator was 3% at ε = 1%, 12% at ε = 0.10%, and 17% at ε = 0.05% (Fig. 5). The light yield loss of the ternary scintillator irradiated with the dose of 10 Mrad was 17% at ε = 0.01% and 6% at ε = 0.10%.

Note that the maximum light yield of the 3HF scintillator is observed at the 3HF concentration of about 1% as for typical ternary scintillators.

Transmittance loss of the 10-cm-thick 3HF scintillator after recovery is comparatively low (~12%) even at the 3HF concentration of 1% (Fig. 6).

To study the radiation effect on the emission capability of a 3HF sample, it was irradiated with a dose of up to 100 Mrad and then used as a secondary fluor in the ternary PS + 1% PTP + 0.01% 3HF scintillator. A comparison of the light yield of this scintillator and a ternary scintillator with 3HF as the secondary fluor that was not irradiated at 100 Mrad did not reveal any noticeable difference. Thus, the scintillator light yield loss is mainly caused by the damage of the scintillator base.

High radiation hardness was exhibited by PVT-based scintillators with the pTP and 3HF fluors irradiated with ^{60}Co γ rays with a dose of 10 Mrad at a dose rate of 0.08 Mrad/h rapidly recovered in the argon atmosphere at a temperature of 50°C [19]. The investigations showed that pTP and 3HF are radiation-hard (including recovery) at doses up to 10 Mrad, and the loss in the scintillator is only due to the transmittance loss of the scintillator's PVT base itself.

Scintillator base materials (PMMA, PS, PVT). Radiation damage caused by γ rays with the dose of 10^3–10^5 Gy at the dose rate of 30–1000 Gy/h in thin SCSF-38 polystyrene samples, PMMA-based wavelength shifters (Y7 UVA, K27 UVA), light guides

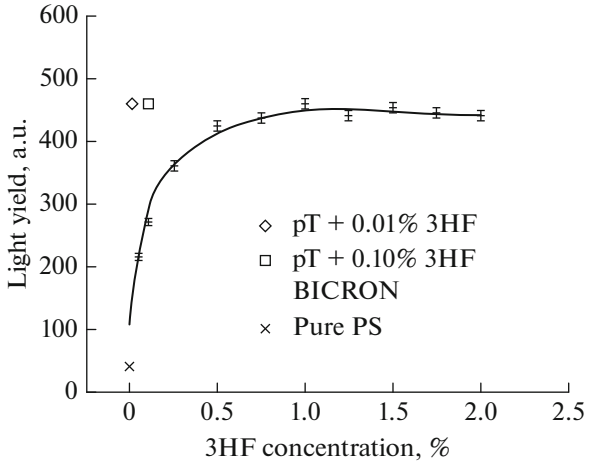

Fig. 4. Light yield of the nonirradiated 3HF scintillator as a function of the 3HF concentration [18]. Also shown are light yields of the Bicron 408, pure PS-based, and ternary scintillators (PS + 1% pTP + 0.1% 3HF) and (PS + 1% pTP + 0.01% 3HF).

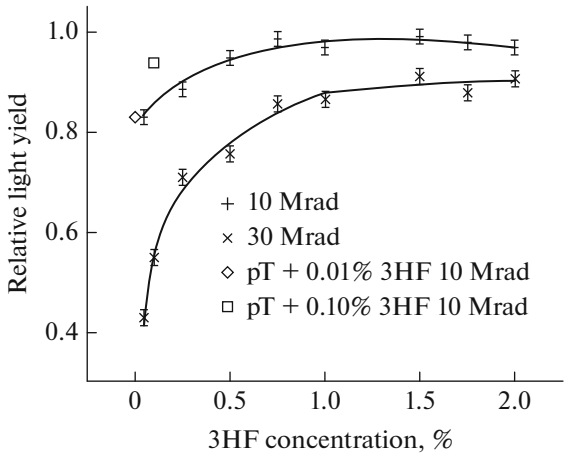

Fig. 5. Ratio of the 3HF scintillator light yield measured after recovery to the light yield measured before irradiation as a function of the concentration of 3HF irradiated with the doses of 10 and 30 Mrad, and the same for the ternary scintillators irradiated with a dose of 10 Mrad [18].

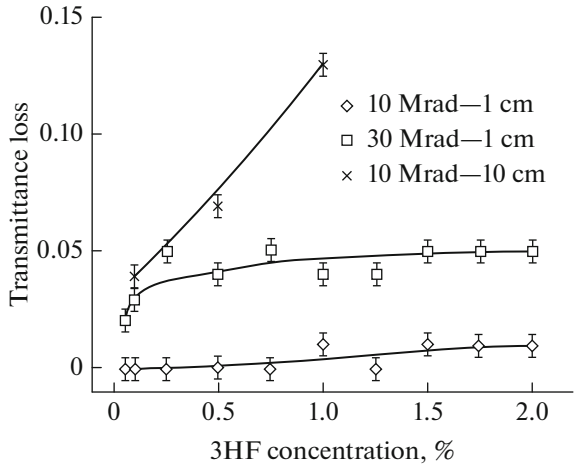

Fig. 6. Transmittance loss at λ = 530 nm for the 3HF scintillator with the thickness of 1 cm (two lower curves) and 10 cm (upper curve) irradiated with a dose of 10, 30 Mrad as a function of the 3HF concentration measured after recovery [18].

(GS218, GS233 UVA, XT20070 UVA) with and without UVA (ultraviolet absorbers to suppress Cherenkov light), and AFS scintillator (PMMA + 10% naphthalene + 1% butyl-PVD) was investigated in [16]. The XT20070 light guide was PMMA extruded. It was shown that after irradiation SCSN-38 recovered fast in the O_2 atmosphere and very slowly in inert gases (N_2, CO_2, Ar). An exception was the AFS scintillator, which recovered only in inert gases.

The time dependence of the recovery zone thickness (z) for SCSN-38, Y7, K27 and GS218, GS233 UVA, XT20070 UVA is well described by the formula $z^2 = \acute{\alpha}t$. The dependence of z^2 on time for SCSN-38 and K27 WLS after their short-time irradiation with 24 kGy is shown in Figs. 7a and 7b, respectively. Recovery of SCSN-38 in the air proceeds much faster than that of K27 WLS (the curve in Fig. 7a and curve *2* in Fig. 7b), which recovers in O_2 faster than in dry air (Fig. 7b, curves *1*, *2*).

The recovery rate depends on the environment, scintillator material, and number of radicals produced by the radiation. Recovery of SCSN-38 polystyrene takes 40 h in dry air and almost half a year in an inert medium. It proceeds faster in O_2 than in dry air (curves *4*, *5*, *6*) and much slower in the inert atmosphere (N_2, Ar, CO_2) (curves *1*, *2*, *3*) than in O_2 and dry air (Fig. 8a). The residual irrecoverable damage level is 5–10% of the level observed immediately after the irradiation.

The PMMA-based K27 WLS recovers in O_2 for more than a year. This is because the concentration of radicals in PMMA is 60 times higher than in PS, and, in addition, the diffusion coefficient of O_2 in PMMA is ten times smaller than in PS [20].

Scintillators with the PMMA base and K27 and Y7 fluors exposed to ^{60}Co γ rays with 24 kGy showed great radiation damage immediately after irradiation, which affected the behavior of their decay length and recovery process (Fig. 8b) [16]. Decay lengths of scintillators with these fluors changed from 90 cm (before irradiation) to 9 cm (after irradiation), and after 583 days of recovery in the air they were 37 cm for K27 and 48 cm for Y7. This indicates that Y7 is more radiation resistant than K27.

In the scope of the upgrade of the ATLAS Tile Calorimeter radiation hardness investigations were carried out for scintillators of various manufacturers [21]:

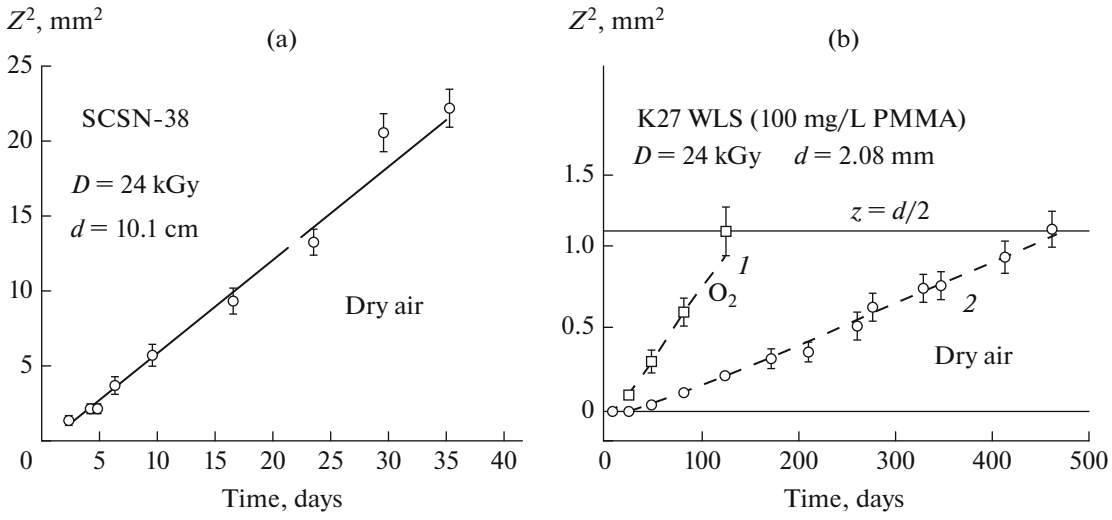

Fig. 7. Recovery of the SCSN-38 (a) and K27 WLS scintilltors (b) after short-time irradiation with the dose of 24 kGy. WLS (*1*) was irradiated in Ar and held in O_2 (P = 800 mb), and WLS (*2*) and SCSN-38 were irradiated and held in dry air (160 mb O_2 + 640 mb N_2) [16].

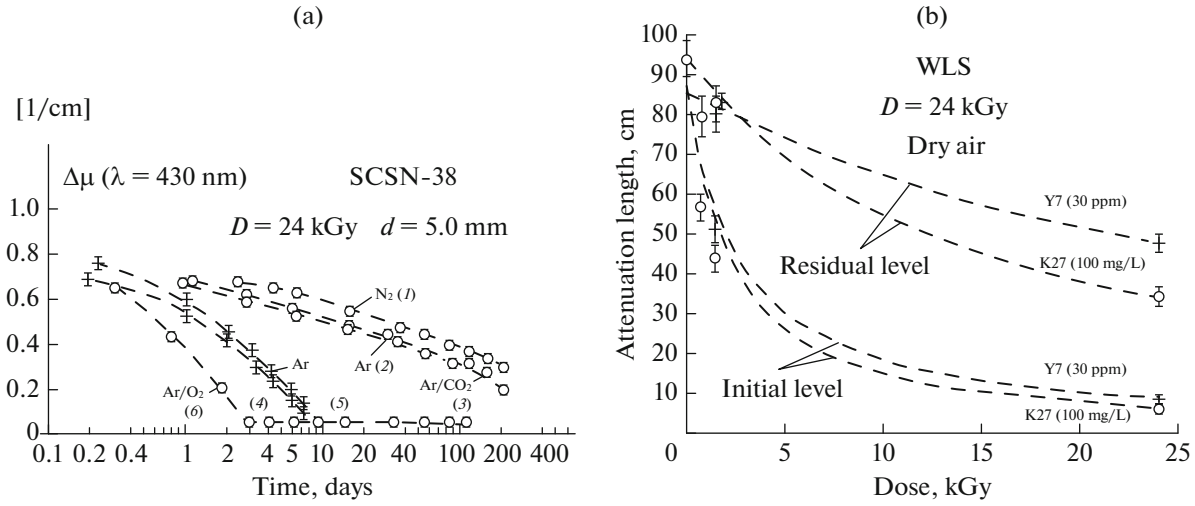

Fig. 8. Recovery of SCSF-38 in different gases. Dependence of the additional absorption coefficient Δμ on time. Experimental conditions: irradiation and storage of SCSF-38 in N_2 (*1*), Ar (*2*), and dry air (*4*). Samples 3, 5, and 6 were irradiated in Ar and stored in CO_2 (*3*), dry air (5), and O_2 (a). Dependence of the attenuation length of the PMMA-based scintillators with the Y7 and K27 fluors at their different concentrations on the radiation dose (b) [16].

IHEP (Protvino) [22], ISMA (Kharkov) [23], Bicron [24], and ELJEN [25]. The Protvino and ISMA (denoted as Dubna in Table 6) scintillators were made of PS, and scintillators of the other two manufacturers were made of PVT. During the upgrade, the scintillators of the MBTS detector located in the gap between the central and extended barrels of the Tile Calorimeter are planned to be replaced with more radiation-hard ones.

It was of great interest to study characteristics of the EJ 200, EJ 208, and EJ 260 (ELJEN) scintillators, which were not previously used in ATLAS spectrometer, and compare them with the characteristics of scintillators from other manufacturers. The Protvino and Dubna scintillators were used in the Tile Calorimeter and the MBTS detectors respectively. All scintillators emit light in the blue region except the EJ 260 scintillator, which emits light in the green region.

Scintillator samples in the form of 5 × 5 × 0.35-mm plates were irradiated with 6-MeV protons at very high doses (0.8, 8, 25, 80 MGy). The data on transmittance loss for all investigated scintillators at different radiation doses and the wavelength of 420 nm are summarized in Table 6.

At high radiation doses (>8 MGy) the highest transmittance loss is suffered by PS-based scintillators and BICRON, and the lowest, by EJ scintillators (Table 6). Measurements of the EJ 208 scintillator transmittance immediately after irradiation in relation to the wavelength at different doses are shown in

Table 6. Transmittance (*T*) loss of scintillators at different radiation doses (wavelength λ = 420 nm) [21]

Scintillator	Dose, MGy	% *T* loss	Scintillator	Dose, MGy	% *T* loss
EJ 200	80	42.9	Protvino	80	60.8
	25	28.6		25	34.8
	8	14		8	7.4
	0.8	3.9		0.8	3.3
EJ 208	80	29.1	Dubna	80	51.3
	25	14.9		25	35.1
	8	4.7		8	26.6
	0.8	2.5		0.8	5.5
EJ 260	80	44.8	Bicron	80	45.5
	25	15.5		25	39.5
	8	14.3		8	11.5
	0.8	6.6		0.8	8.7

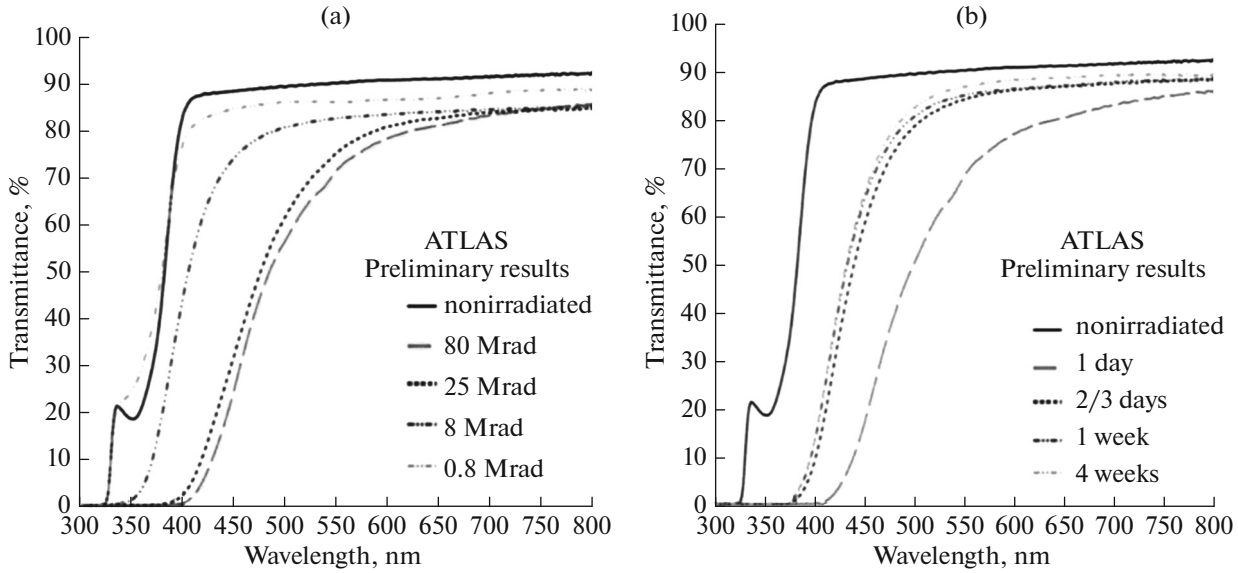

Fig. 9. Transmittance of the EJ208 scintillators as a function of the wavelength at different radiation doses (a) and time after irradiation (b) [21].

Fig. 9a. As the dose increases, the transmittance decreases, and the spectra shift to the region of longer waves. A similar dependence is observed for the EJ260 scintillator.

Of all EJ scintillators, the best are EJ208 in transmittance at all radiation doses and EJ260 in recovery time (Table 7). The EJ 260 and EJ 208 scintillators recover their transmittance better than EJ 200, and, which is important, they have appreciably recovered in the first two or three days while in the next four weeks the recovery is very insignificant (Fig. 9b and Table 7).

In the scope of the upgrade of the CMS HE hadronic calorimeter, light yield, light collection efficiency, and temporal characteristics of ELJEN scintillators were investigated using μ-meson beams with the energy of 150 GeV in H2 beamline of the SPS (CERN) [25]. The main objective was to study a possibility of replacing SCSN-81 scintillators used in the CMS HCAL. In making a choice, account was taken of the fact that scintillators with a higher fluor concentration and with the emission spectrum shifted to the green region exhibit higher radiation hardness [21]. The decision was in favor of EJ-200 P2 with different primary fluors and EJ-200 2X with twice the concentration of fluors whose spectrum is shifted to the green region (Table 8 [26]).

Table 7. Transmittance loss $\Delta T(\%)$ of EJ scintillators in relation to the time after irradiation with the doses of 8 MGy and 25 MGy [21], where ΔT is the transmittance loss in percent defined as a difference in transmittance loss in percent between nonirradiated and irradiated samples

Dose, MGy	Sample	ΔT, % (1 day–1 week)
25	EJ 200	30.38
	EJ 208	37.06
	EJ 260	6.45
		ΔT, % (1 day–4 weeks)
8	EJ 200	15.05
	EJ 208	5.92
	EJ 260	2.22

The results of the investigations were compared to the characteristics of the SCSN-81 scintillator and commercially available EJ-200. The investigated scintillating tiles were 100 × 100 × 4 mm^3 in size. Light from them was collected by Kuraray Y11 or O-2 WLS fibers connected to SiPMs. The emission peak of O-2 fibers is 538 nm. The fibers were embedded in a σ-shaped groove on the tile surface. The light yield of EJ-200 2X and EJ-260 was lower than that from SCSN-81 because the increased concentration of fluors in EJ-200 2X leads to increasing light self-absorption in the fluor itself. The lower light yield in EJ-260 is partially due to its lower transparency than that of EJ-200 and lower quantum efficiency of SiPMs in the green region than in the blue region typical of EJ-200.

However, temporal characteristics of EJ-200 P2 and SCSN-81 are almost identical. Green EJ-260 scintillators are slower than blue scintillators by approximately 5 ns, which falls within the bunch duration of 25 ns at the LHC.

Thus, the analysis of the light yield and temporal characteristics of the investigated scintillators shows that increased concentrations of fluors and switching to fluors with green-region emission spectra seem to be a promising way.

Table 8. Main characteristics of scintillators investigated in [26]

Material	Base	Emission peak, nm	Notes
SCSN-81	PS	440	Used at CMS HCAL, no longer manufactured
EJ-200	PVT	425	Commercial scintillator ELJEN equivalent to BC-408
EJ-200 2X	PVT	425	Special version of EJ-200 with primary fluor concentration twice as high as in its commercial version
EJ-200 P2	PVT	425	Special version of EJ-200 with different primary fluors
EJ-260	PVT	490	Green spectrum scintillator with decay time of 9.3 ns whereas decay time of a blue spectrum scintillator is about 2 ns

Table 9. Light yield (LY) and recovery time of the PEN and PET scintillators

Scintillator	Primary LY, %		Recovered LY, %		Recovery time, days	
	1.4 Mrad	14 Mrad	1.4 Mrad	14 Mrad	1.4 Mrad	14 Mrad
PEN	71.4	46.7	85.9	79.5	5	9
PET	35.0	12.2	93.5	80.0	22	60

Existing and projected accelerators need scintillators that meet strict requirements not only on radiation hardness but also on temporal characteristics. Of particular interest is also the cost of scintillators since a great deal of them have to be used in experiments. For example, the ATLAS Tile Calorimeter comprises about 500000 scintillating tiles. In this connection, noteworthy are studies of radiation hardness and temporal characteristics of polyethylene naphthalate (PEN) and polyethylene terephthalate (PET) [27]. These materials are also widely used in production of plastic bottles, various containers, etc. The studied PET and PEN samples measured 100 × 100 × 2 mm and 100 × 100 × 1 mm respectively.

These materials have good scintillating properties. Emission spectra of PEN and PET scintillators are in the blue region with the peak wavelengths of 450 and 350 nm and light yields of 10500 and 2200 photons respectively. Radiation tests of PEN and PET scintillators were performed using ^{137}Cs γ rays with the doses of 1.4 and 14 Mrad. The light yield losses of the scintillators in relation to the time measured for 50 days after irradiation are shown in Fig. 11.

Table 9 presents light yields of both scintillators after irradiation with 1.4 and 14 Mrad and after recovery and their recovery times. The light yield loss in PEN immediately after irradiation with 1.4 and 14 Mrad is 28.6 and 53.3% respectively, and in PET it is 65 and 87.8%. Residual light yields after recovery of both scintillators irradiated with a dose of 14 Mrad are almost identical, and the recovery time of PEN is much shorter than that of PET.

Temporal characteristics of the PEN and PET scintillators were studied in comparison with those of the SCSN-81 scintillator used in the CMS experiment at the LHC. Their respective response times turned out to be 27.12, 6.884, and 10.56 ns, i.e., the response time of PET is much shorter than that of PEN.

Recovery investigations of the PEN (Scintirex Brand Scintillator) [28], ES (epoxy elastomer doped with pTP), EJ-260 (ENJ), and EJ-260 (EJ2P) scintillators irradiated with γ rays from the ^{137}Cs source with the doses of 100 kGy (PEN) and 78 kGy (ES, EJ) were performed in [29]. PEN and ES are characterized by the blue emission spectrum, and EJN and EJ2P, by the green one. The investigated PEN samples measured 5 × 5 × 0.1 cm, and three others were a few cm^2 in cross section and 1 cm thick.

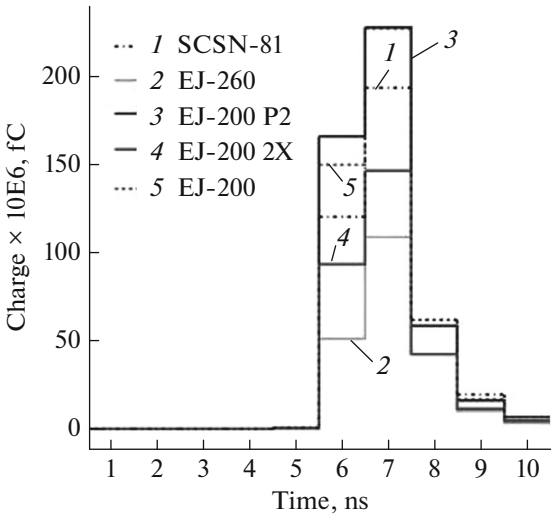

Fig. 10. Distribution of the integrated charge from the scintillators in the time interval of 25 ns (over the full data set).

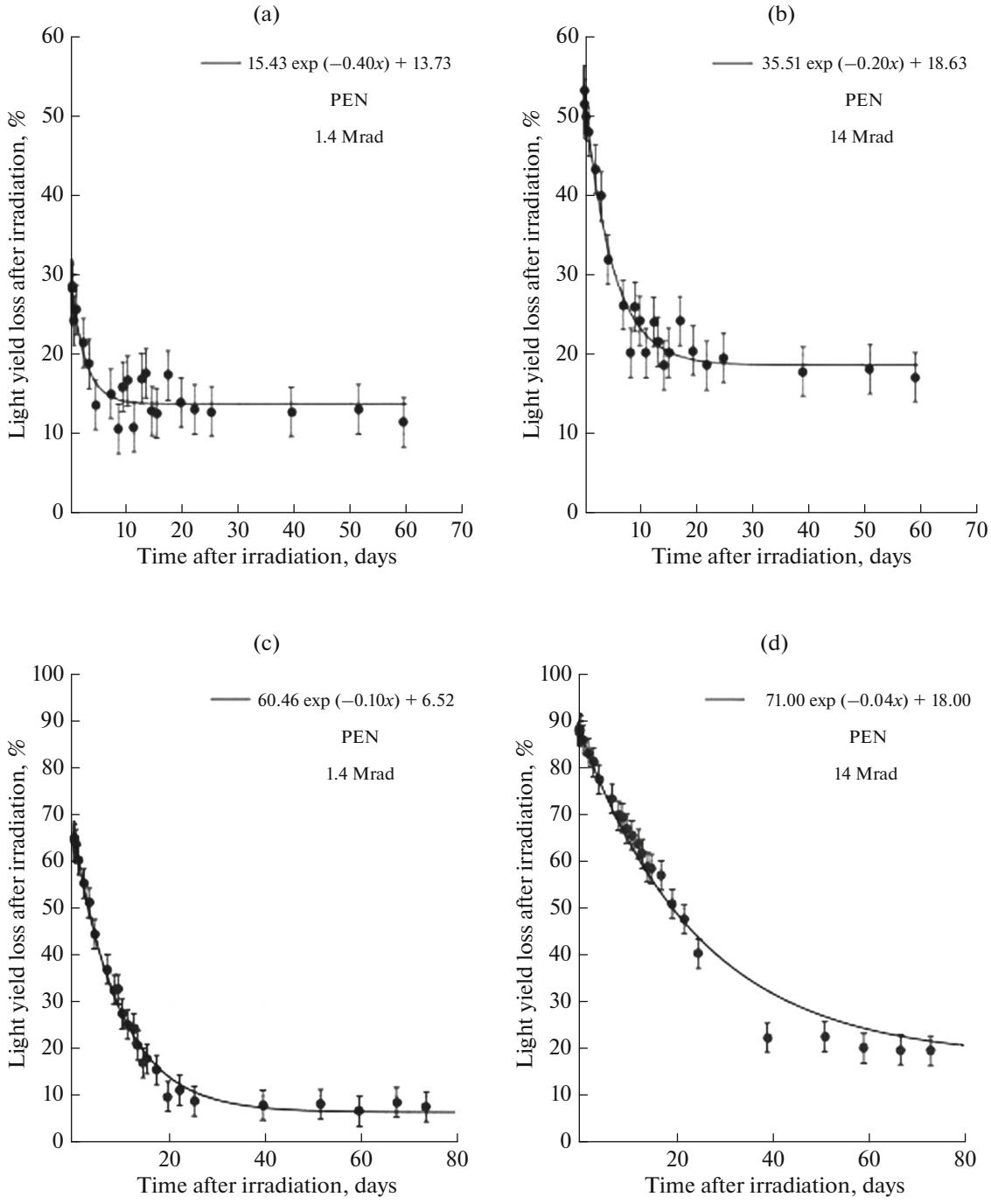

Fig. 11. Light yield loss of PEN (a, b) and PET (c, d) irradiated with γ rays from the ^{137}Cs source with the doses of 1.4 and 14 Mrad, respectively, for 50 days after irradiation.

After irradiation, two PEN samples were kept in a dark box, and one was placed in the RGB LED matrix like all the other samples. Seven days after irradiation the PEN samples kept in the dark box (dark box) recovered to 40% and the third sample with the LED matrix recovered to 72% of the level before irradiation. The corresponding recovery parameters of the ES scintillators were 56 and 46%. The RGB LED did not produce any noticeable effect on the recovery of the EJ2P and EJN samples (Table 10).

Table 10 summarizes data on recovery of ES, EJN, and EJ2P scintillators in relation to time t fitted by the function

$$f(t) = \mathbf{a}\exp(-\mathbf{b}t) + \mathbf{c}, \quad (1)$$

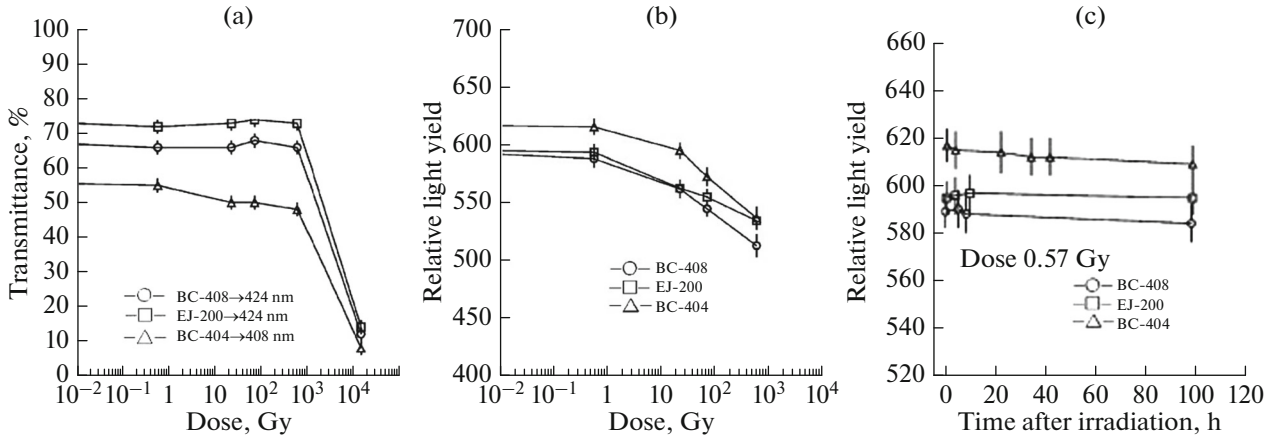

Fig. 12. Transmittance of the BC-408, BC-404, and EJ-200 scintillators as a function of the absorbed dose at their typical emission wavelengths, (a) variation in the relative light yield of the scintillators as a function of the absorbed dose, (b) and the time after irradiation (c) [30].

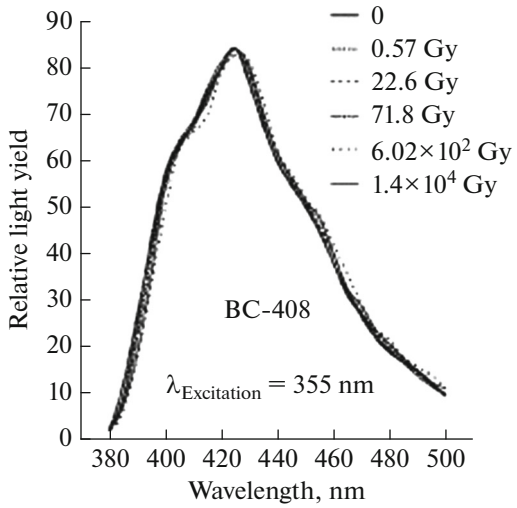

Fig. 13. Emission spectra of the BC-408 scintillators before and after irradiation [30].

where **a** is the difference between the initial (immediately after irradiation) and residual damage level, **b** is the recovery constant, and **c** is the residual damage level.

Thus, the RGB LED matrix with the blue emission spectrum turned out to be quite effective for improving recovery of the blue scintillators PEN and ES while the green scintillators EJ2P and ENJ need other LEDs for their recovery.

Recovery investigations of the BC-408, BC-404, and EJ-200 fast scintillators often used for time measurements were performed using ^{60}Co γ rays with doses of (0.57–1.4) × 10^4 Gy [30]. Transmittance of these scintillators when irradiated with a dose below 600 Gy hardly change. Its substantial change is observed only at doses >1.4 × 10^4 Gy and a dose rate of 52.7 Gy/min (Fig. 12a).

All samples exhibit a very small decrease in the light yield after irradiation with a dose below 50 Gy, and at the dose of 600 Gy the light yield loss was 14.1% in BC-408, 13.4% in BC-404, and 10.6% in EJ-200 (Fig. 12b). Almost no changes are observed in the light yield of the scintillators after their irradiation with 0.57 Gy for 100 h (Fig. 12c).

The shape and position of the emission peak in the spectrum of three scintillators did not change at all radiation doses, which indicates that the fluor-light generation mechanism is not destroyed at the doses under consideration. Figure 13 shows BC-408 emission spectra.

Dependence of radiation hardness on the dose rate. Radiation damage of scintillators depends not only on the absorbed dose but also on the dose rate. The effect of the dose rate on the light yield was investigated in the SCSN38, SCSN81, and Bicron 499-35 scintillators made of PS (the first two) and PVT (the third) [31]. Their light yields were measured at the doses rates of 2.3 krad/h to 1.5 Mrad/h and absorbed dose of 10 Mrad.

Table 10. Parameters of the function $f(t)$

Sample	**a**	**c**	**b**, 1/days
ES RGB	56.3 ± 2.4%	30.7 ± 1.6%	0.22 ± 0.03
ES dark box	45.7 ± 2.5%	44.1 ± 1.9%	0.18 ± 0.03
EJN RGB	24.0 ± 2.2%	6.92 ± 0.7%	0.64 ± 0.16
EJN dark box	21.1 ± 1.8%	15.9 ± 0.6%	0.50 ± 0.11
EJ2P RGB	26.9 ± 3.1%	15.2 ± 0.9%	0.75 ± 0.22
EJ2P dark box	26.5 ± 2.2%	13.7 ± 0.7%	0.62 ± 0.14

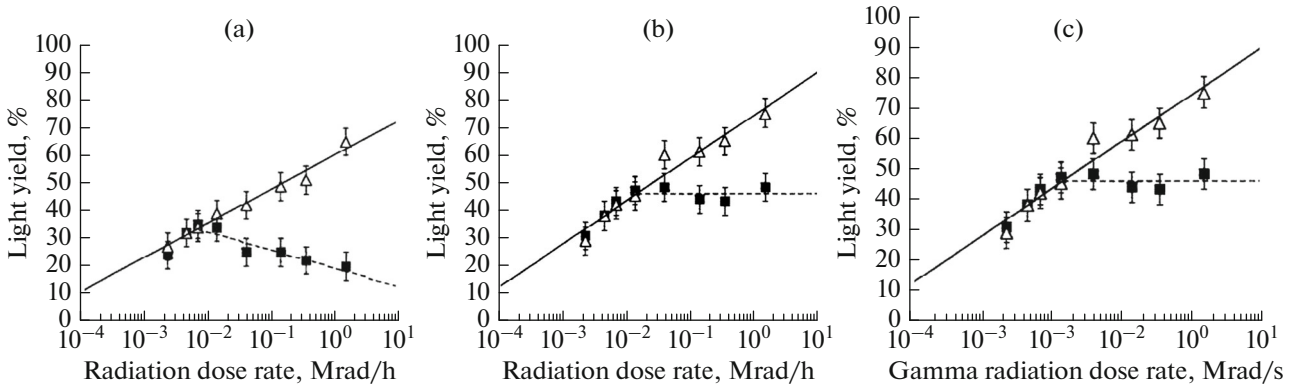

Fig. 14. Light yield of the SCSN-38 (a), BC-499-35 (b), and SCSN-81 (c) scintillators as a function of the radiation dose rate immediately after irradiation (squares) and after seven days of recovery (triangles) [30].

The results of the measurements immediately after irradiation and seven days later are shown for the three scintillators in Figs. 14a–14c by black and white squares and triangles. It is seen that the light yield considerably decreases with decreasing dose rate. On the semilog straight line describing light yield immediately after irradiation there is the divergence point below which the light yield of all scintillators drops with decreasing dose rate while above this point it either decreases (SCSN-38), or remains unchanged (SCSN-81), or increases (Bicron 499-35). The authors of the study explain this by the difference in O_2 penetration into the scintillators and by the mobility of molecular chains of the scintillators.

Note that below the divergence point the light yields of the scintillators seven days after irradiation are the same as immediately after irradiation.

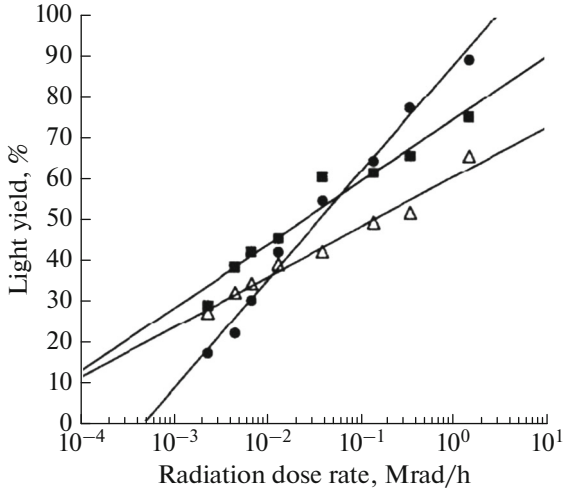

Fig. 15. Light yield of the scintillators after seven days of recovery as a function of the radiation dose rate: triangles are SCSN-38, squares are SCSN-81, and circles are Bicron 499-35 [31].

Light yields of SCSN-38, SCSN-81, and Bicron 499-35 after their recovery are well described by a semi-log straight line with the slope angle depending on the scintillator material and irradiation conditions (Fig. 15). In some cases, this dependence describing measurements of light yield of a scintillator at high dose rates may help estimate the expected light yield of the same scintillator at low dose rates with the same absorbed dose.

Radiation hardness investigations of the SCSN-81 and BC408 scintillators used in the HE calorimeter, the high radiation CMS hadronic calorimeter, were performed using the LHC proton beam with the energy of 8 TeV at the integrated luminosity of 23.3 fb^{-1} and with very low dose rates of 10^{-4}–0.1 krad/h [32]. In addition, these scintillators were irradiated with ^{60}Co γ rays at the dose rate of 0.28 krad/h and absorbed dose of 300 krad.

Light yields of the scintillators were measured before and six days after irradiation. The results are shown in Fig. 16 as dependences of the constant D on the radiation dose rate, where D is the constant in the formula that describes light yield of scintillators as a function of the radiation dose d [32]

$$L(d) = L_0 \exp(-d/D). \quad (2)$$

The above results indicate that the light yield considerably decreases with decreasing dose rate. A comparison of these results with the data obtained at high γ dose rates [31] showed that both data sets functionally agree rather well.

The effect of the dose rate on the light yield stems from diffusion of O_2 into the scintillator, which is described by the power-law function [16]. Note that the O_2 diffusion rate is mainly determined by the scintillator material; for example, in nonirradiated PS it is 13 times higher than in PVT [33].

Radiation tests were mainly performed with small scintillator samples a few millimeters to 1 cm thick, and in [34] they were performed with large (19 × 29 ×

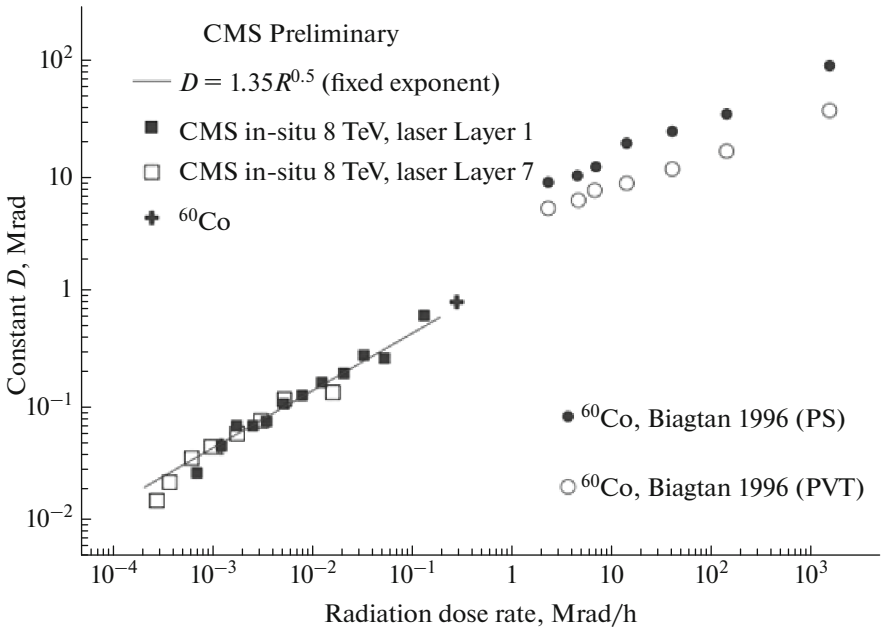

Fig. 16. Dependence of the constant D on the radiation dose rate of 8 TeV protons in irradiation of PS-based scintillators in CMS HE calorimeter layers 1 and 7, filled and open blue squares respectively [32]. The blue cross is the result obtained in irradiation with γ rays from the ^{60}Co source [32]. Also shown are the data from ^{60}Co γ irradiation of the PS- and PVT-based scintillators, filled blue and open red circles [33].

120 cm) samples of PS and ternary PS-based scintillator doped with 0.4% PPO and 0.04% POPOP, which were exposed to ^{60}Co γ radiation with doses of 1 to 10 kGy and dose rates of 0.1 and 85 kGy/h.

At low dose rates transmittance and light yield, losses (Figs. 17a, 17b) are larger than at high dose rates, which is due to different processes of color center formation and light absorption in these color centers at the interaction of O_2 with radicals. As the radiation dose increases, the transmittance loss, signal intensity loss (Fig. 17c), and mechanical strength loss (Fig. 17d) develop slower. However, the positon of the peak in the emission spectrum did not change with increasing absorbed dose.

Transmittance loss in the scintillator doped with 0.4% PPO + 0.04% POPOP at doses >2 kGy turn out to be higher than in pure polystyrene (Fig. 18a). Post-irradiation recovery of the samples proceeds according to the exponential law and reaches the residual level of 5% within about a month (Fig. 18b).

Radiation hardness investigations with neutron beams. Investigation of PS-based scintillators irradiated with neutrons is of great practical interest because many neutrons are produced at modern accelerators in electromagnetic and hadronic calorimeters and other parts of accelerators. At the LHC, more than 10^{15} neutrons/cm^2 are expected in its very high radiation areas for a year of operation [4].

Radiation hardness investigations of the SCSN-38, pure PS and PMMA GS218 scintillators were performed using neutron beams from the BR1 nuclear reactor (Belgium) and from the PTB synchrotron (Braunschweig, Germany) [35]. Scintillator samples measured 10 × 10 mm and were 4(5) mm thick. At the PTB accelerator neutrons were produced in the reaction ^{9}Be(d, n) ^{10}B. Parameters of neutron beams were as follows:

PTB: fluence is 7×10^{14} neutrons/cm^2, γ background is 7% of the total dose, and average neutron energy is 5.2 MeV.

BR1: fluence is 1.9×10^{15}–4.4×10^{16} neutrons/cm^2, γ background is 5%, and neutrons are 86.5 thermal, 5.4 epithermal, and 8.6% fast [35].

The transmittance of the scintillators T can be described by the formula

$$T(\lambda) = T_0(\lambda)\exp(-\mu(\lambda)t), \quad (3)$$

where μ is the absorption coefficient, t is the scintillator thickness, and T_0 is the transmittance before irradiation. For irradiated materials, the radiation-determined absorption coefficient Δμ is used, which is equal to the difference between the absorption coefficients of the irradiated and recovered scintillators.

In the wavelength region λ = 380–400 nm, where absorption of the BDB activator is high, damage from γ radiation with the doses of 154 and 200 kGy is larger than from neutrons (Fig. 19a), and at low doses of 5.2 and 7.0 kGy damage from neutrons is almost five times larger than from γ rays (Fig. 19b).

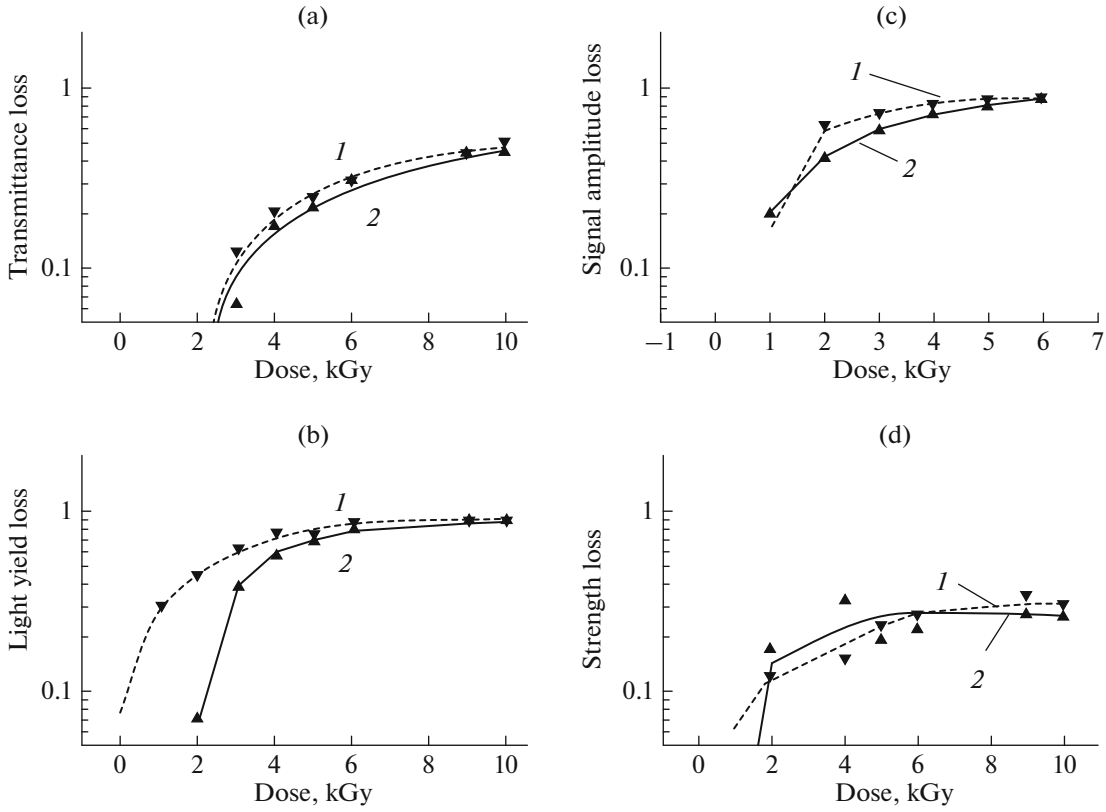

Fig. 17. Scintillator transmittance (a), light yield (b), signal amplitude (c), and strength limit (d) losses as a function of the absorbed dose at a low (0.1 kGy/h) and a high (8.5 kGy/h) radiation dose rate, curves 1 and 2 respectively [34].

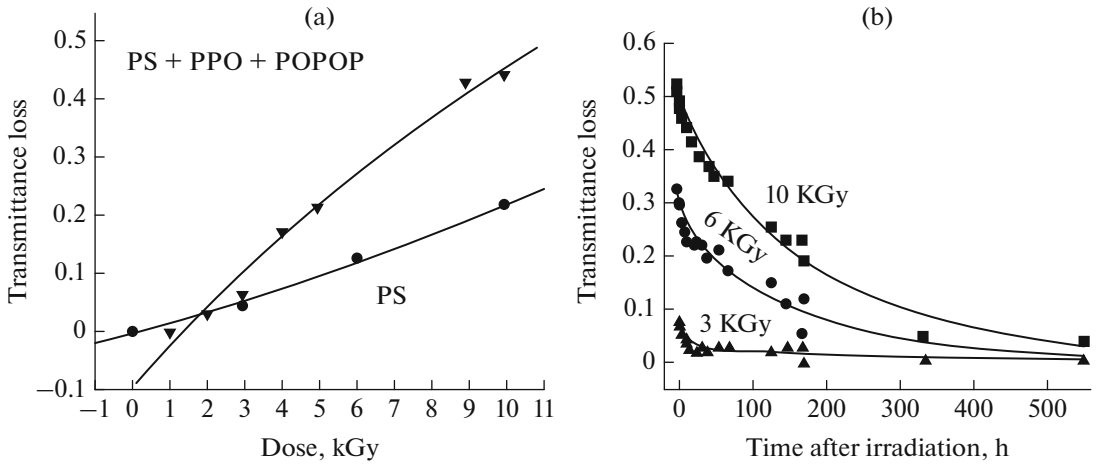

Fig. 18. Transmittance loss of pure polystyrene and the scintillator + 0.4% PPO + 0.04% POPOP as a function of the absorbed dose (a). Recovery of the scintillator light transmission as a function of time after irradiation with different doses and at λ = 440 nm (b) [34].

The data on the dependence of $\Delta\mu$ on the neutron and γ radiation dose for PS, SCSN38, and PMMA are summarized in Figs. 20a and 20b.

In PS and SCSN-38 neutrons cause greater damage than γ rays by about a factor of three (Fig. 20a), while in PMMA γ rays produce 1.5 times more damage than neutrons (Fig. 20b). In organic scintillators the cross section for neutron–proton interaction is larger than for γ-ray absorption, therefore, protons arising from elastic neutron scattering in PS cause larger damage than in PMMA.

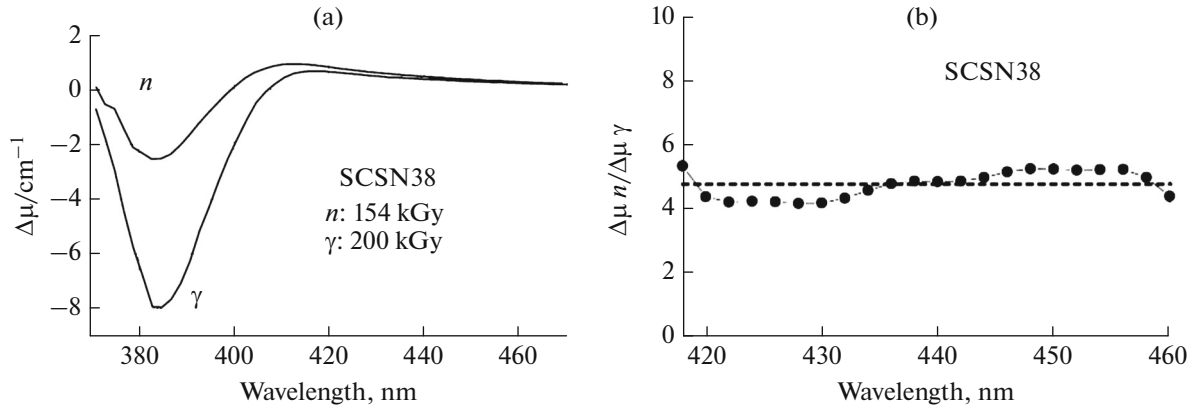

Fig. 19. Dependence of the absorption coefficient Δμ on the wavelength for SCSN38 irradiated with neutrons and γ rays with the doses of 154 kGy and 200 kGy (a); neutron-to-γ Δμ ratio for SCSN38 irradiated with neutrons and γ rays with the doses of 5.2 kGy and 7.0 kGy (b) [35].

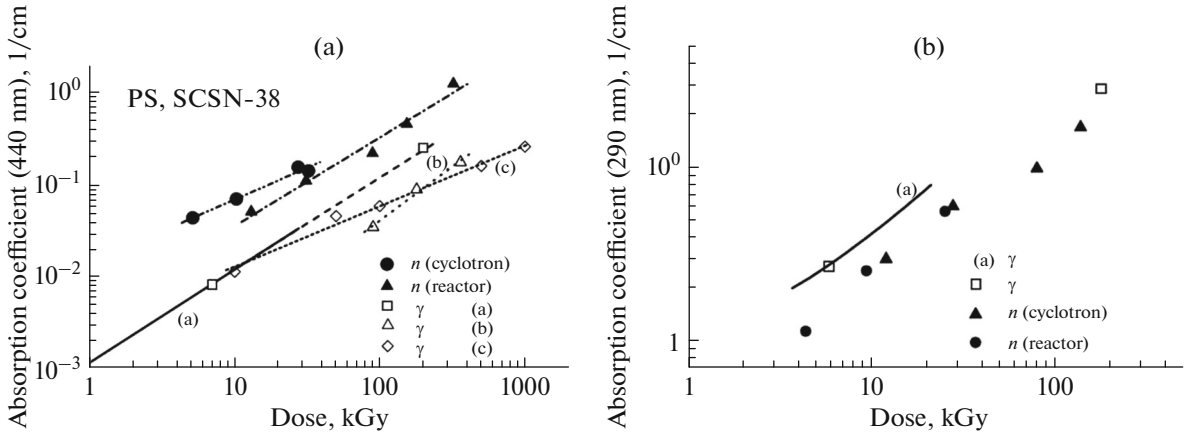

Fig. 20. Dependence of the absorption coefficient Δμ on the neutron and γ-ray radiation dose for PS and SCSN-38 at λ = 440 nm (a) and PMMA at λ = 290 nm (b) [35].

To improve light collection and increase radiation hardness of scintillating tiles used in high-radiation zones of accelerators, e.g., in the CMS calorimeters, it is proposed to replace particular tiles with several strips, collect light from each strip by a WLS fiber embedded in the strip groove, and sum it [36, 37]. This segmentation of a tile into small "finger" strips allows much larger light collection than from a single whole tile. This is because the strip scintillation light travels a shorter distance from its generation point to the WLS fiber and thus its absorption and scattering losses are lower. In addition, a shorter scintillation light path also means a lower probability to be affected by radiation damage.

Measurements of light yields from a 100 × 100 mm^2-tile and from 16 strips 100 × 6 mm^2 irradiated with electrons with doses of 0.5, 1, 5, 10, and 30 Mrad showed that the total light yield from 16 strips could be up to 40% higher than from a tile (Fig. 22a) [36].

The light yield of a whole 60 × 40 × 4-mm SCSN-81 tile was investigated in relation to the dose rate using ^{60}Co γ-ray radiation with the total doses of 250 and 600 krad [37] (Fig. 22b). The light yield showed dependence on the radiation dose rate with a trend to decrease with decreasing dose rate.

Several 60 × 12 × 4 mm BC-408 and EJ-260 finger strips with light-collecting Y11 and O-2M Kuraray WLS fibers, respectively, were exposed to ^{60}Co γ radiation with doses of 5 to 30 Mrad at dose rates of 0.022 to 0.600 Mrad/h at the Institute of Nuclear Problems (Tashkent). Light yields of these strips (in photoelectrons) γ-irradiated with the doses of 20 and 25 Mrad are shown as a function of the radiation dose rate in Figs. 23a and 23b respectively. At low dose rates, the light yield of the scintillators was much lower than at high dose rates (at the same radiation dose).

Silver painting of the fiber end far from the PD improved light collection by a factor of 1.45. Figure 23c shows the light yield of the BC-408 strip with the Kur-

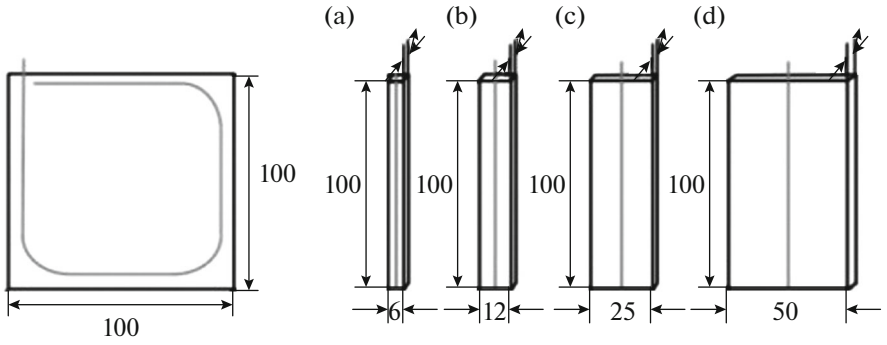

Fig. 21. Tile with dimensions 100 × 100 mm^2 and strips with widths of 6, 12, 25, and 50 mm [36].

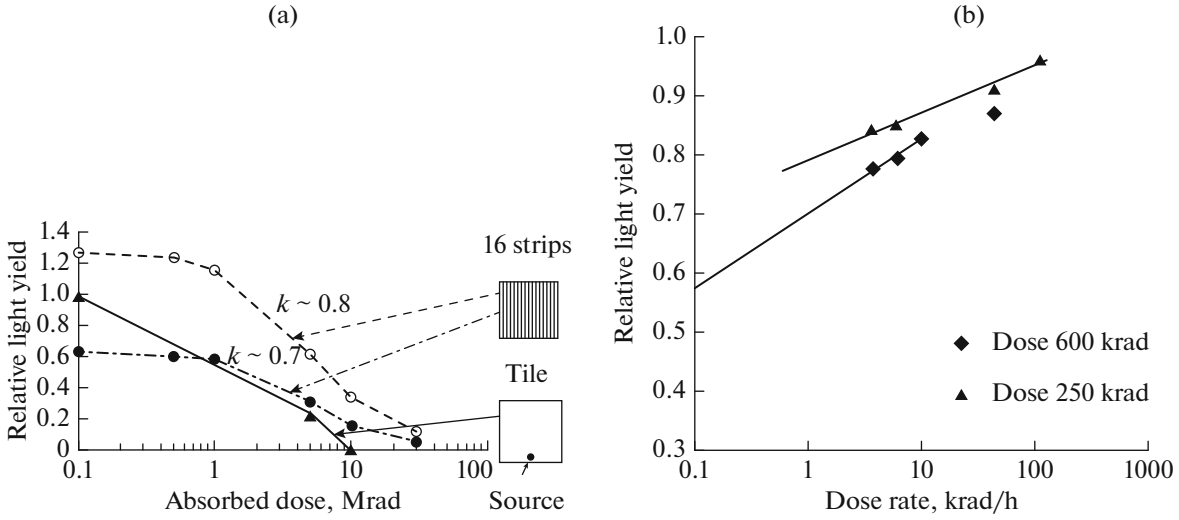

Fig. 22. Relative light yields of different samples calculated on the basis of measurements. The light source was at a distance of ~2 mm from the shifter [36] (a). Relative light yield of the SCSN-81 tile not divided into strips as a function of radiation dose rate [36] (b).

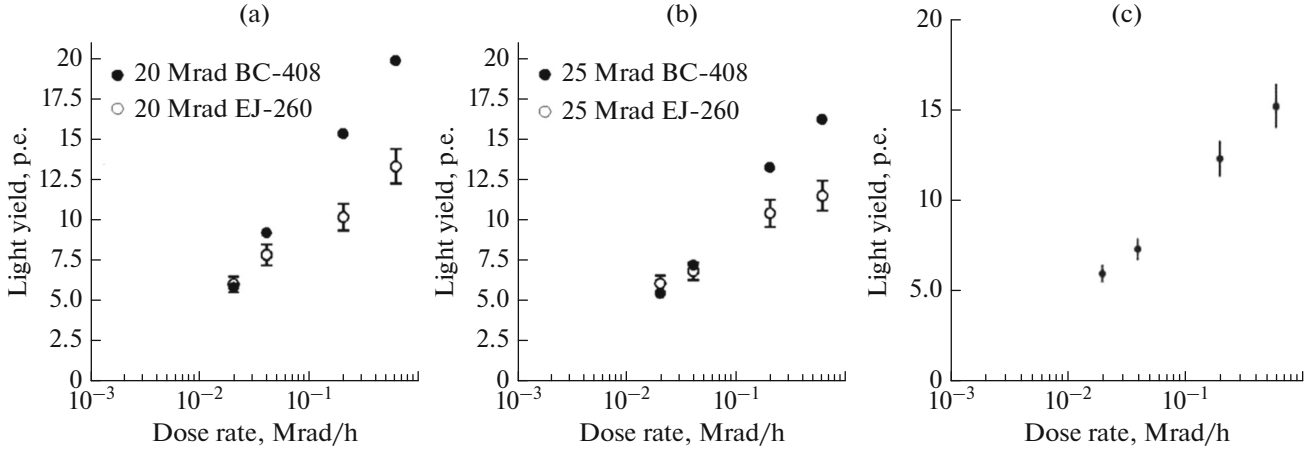

Fig. 23. Light yield from the BC-408 and EJ-260 strips irradiated with γ rays with the doses of 20 Mrad (a), and 25 Mrad (b) and the BC408 strip with the Y11-M fiber irradiated with γ rays with the dose of 25 Mrad (the fiber end face with respect to the PD was painted silver) (c) as a function of the dose rate (average γ energy is 1.5–2 MeV) [37].

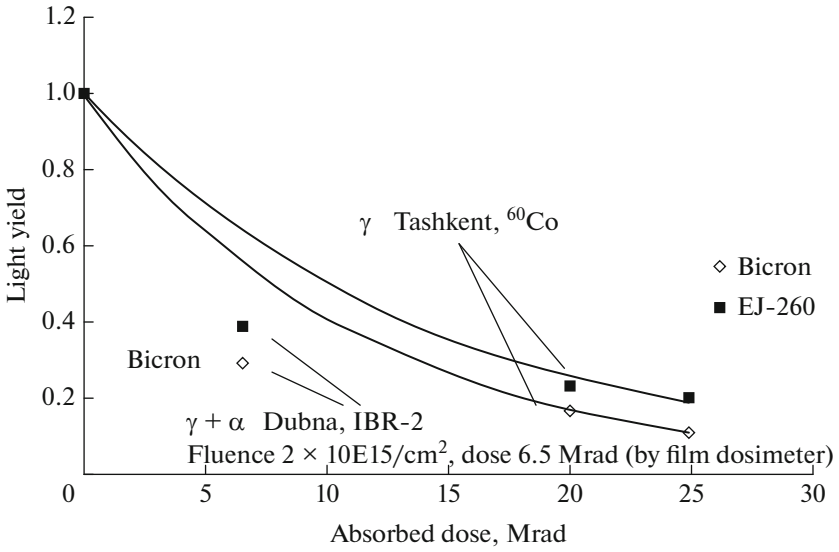

Fig. 24. Relative light yields of the BC-600 and EJ-260 finger strips irradiated with γ rays alone (Tashkent, ^{60}Co) and with a mixed neutron–γ beam (Dubna, IBR -2) [37].

aray Y11-M fiber irradiated with 25 Mrad. The fiber was irradiated with 6-MeV electrons, and its end far from the PD was painted silver. Light yields of this strip (Fig. 23c) and the strip that was irradiated with the same dose of 25 Mrad, while the fiber was not irradiated, and its end was not painted (Fig. 23b) turned out to be almost identical. This means that painting of the fiber end compensates for the light loss caused by irradiation with the dose of 25 Mrad.

Radiation hardness investigations of BC-600 and EJ-260 finger strips were also performed with neutrons from the IBR-2 fast pulsed reactor (JINR), a unique machine producing neutrons fluxes of up to 10^{16} neutrons/cm^2/s [38]. The strips were irradiated with a mixed beam that contained 85% of neutrons and 15% of γ rays with the average neutron energy of ~1 MeV and γ-ray energy of 1.5–2 MeV; the neutron fluence was ~3×10^{15} neutrons/cm^2.

The results of the measurements with neutrons and γ rays at 20 and 25 Mrad are shown in Fig. 24. Light yield loss in neutron-irradiated scintillators is higher than in γ-ray irradiated ones at the same radiation dose of 6.5 Mrad, which corresponded to the fluence of 2.34×10^{15} neutrons/cm^2.

In the scope of the ATLAS spectrometer upgrade, optical and structural changes were investigated in the PVT-based scintillators EJ-200, EJ-208, and EJ-260 (ELJEN) and the PS-based scintillator UPS-928A (ISMA) exposed to a beam of neutrons with the energy of up to 10 MeV and fluence of 1.2×10^{12}–9.4×10^{12} neutrons/cm^2 from the IBR-2 (JINR) [39].

Note that radiation hardness of these scintillators was earlier investigated using proton beams with radiation doses ranging from 0.8 to 80 MGy [21]. It was shown that EJ scintillators exhibited the highest radiation hardness.

At the given neutron fluxes emission spectra (Fig. 25a) and Raman spectra (Fig. 25b) of the irradiated and nonirradiated EJ-200 samples almost coincide, i.e., no structural changes were found in the irradiated samples. Peaks observed in the spectra in the wavelength regions of 300–375 and 375–500 nm correlate with the emission spectra of PS/PVT base and fluors respectively. The same was observed in other ELJEN scintillators as well.

Light yields of the scintillators change little with neutron fluence variation in the interval of $(1–10) \times 10^{12}$ neutrons/cm^2 (Fig. 26).

Radiation hardness of UPS-928A was also investigated at neutron fluences of 3.8×10^{12}–1.8×10^{14} neutrons/cm^2. The light yield of the scintillator at the highest neutron fluences decreased by ~28%. No structural changes and additional emission peaks were found.

3.2. Optical Fibers

Optical fibers (scintillating, wavelength-shifting, and clear) have found wide use in modern accelerator and cosmic ray experiments. The main fiber manufacturers are Kuraray [40] and BICRON [41]. A typical cross section structure of Kuraray round-shaped single-clad (a), round-shaped double-clad (b), and square-shaped single-clad (c) SciFi fibers are shown in Fig. 25. The cladding thickness is about 3% of the core thickness. The fiber core is usually PS, the first (inner) cladding is of PMMA, and the second (outer) cladding is of fluorinated PMMA with the refractive indices of 1.59, 1.49, and 1.42 respectively. This fiber

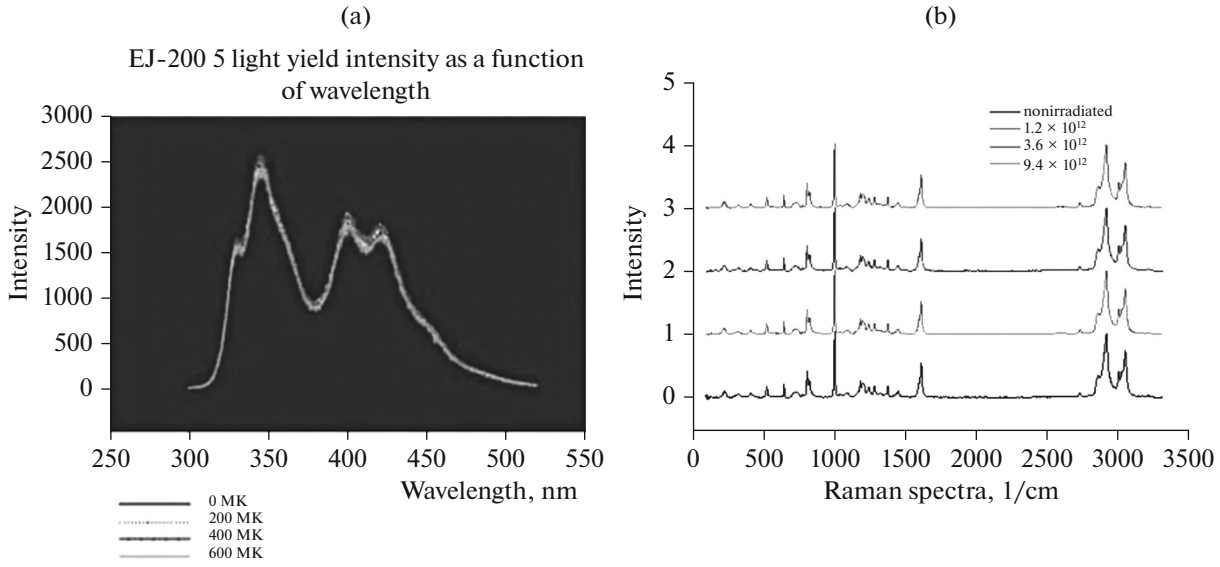

Fig. 25. Emission (a) and Raman spectra (b) for EJ-200 [39].

structure allows efficient light collection and propagation along the fiber due to the total internal reflection in the cladding(s) (Fig. 19). Double-clad fibers allow collecting 50% more light than single-clad ones due to a larger light capture angle (Fig. 26).

Scintillation light propagating along the fiber suffers losses caused by Rayleigh scattering on its various inhomogeneities, self-absorption, and radiation damage. These losses strongly depend on the light wavelength: the less the wavelength λ, the higher the losses. The Rayleigh scattering loss is proportional to $\sim 1/\lambda^4$; therefore, photons with shorter wavelengths are considerably absorbed while photons with longer wavelengths propagate with lower losses.

The amount of scattering and self-absorption losses depends on the fiber core material and the value of the Stokes shift of the fluors, i.e., the difference between the peaks of the emission spectra of primary fluors and the absorption spectra of secondary fluors.

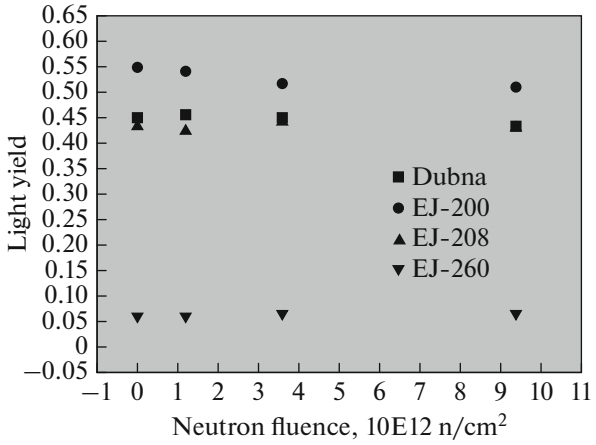

Fig. 26. Light yield of the EJ-200 scintillator as a function of the neutron fluence [39].

In fiber material affected by radiation radicals are produced, which act as light centers, causing absorption and scattering of scintillation light. Radiation damage loss was studied in many publications, some of which will be considered below.

In addition to scintillating fibers, clear optical fibers are often used, which are fibers without fluors and in which photons propagate with lower losses. The CF attenuation length is more than 10 m, which almost three times larger than the SciFi attenuation length. Clear fibers have better mechanical properties than SciFi fibers. In addition, as will be shown below, clear fibers are more radiation-hard than scintillating fibers.

In modern experiments, optical fibers should have good mechanical properties (flexibility) because they are embedded in grooves (in tiles) with small curve radii. Good flexibility is exhibited by Kuraray *S* type fibers, because molecular structures of their core are oriented along the fiber axis. In this connection, it is of great interest how Kuraray *S* type and clear fibers behave in terms of the parameter *S* and the curve radius under high radiation loads.

Scintillating fibers (SciFi) and clear fibers (CF). Scintillating fibers are widely used in very high radiation accelerator areas, being employed in various processes, such as luminosity measurements by the ALFA detector at the LHC [42], spatial-temporal separation of particles by the fiber hodoscope at COMPASS [43], time-of-flight separation of particles at MUSE [44], determination of particle track coordinates at D0 [45], LHCb [46, 47], etc. An

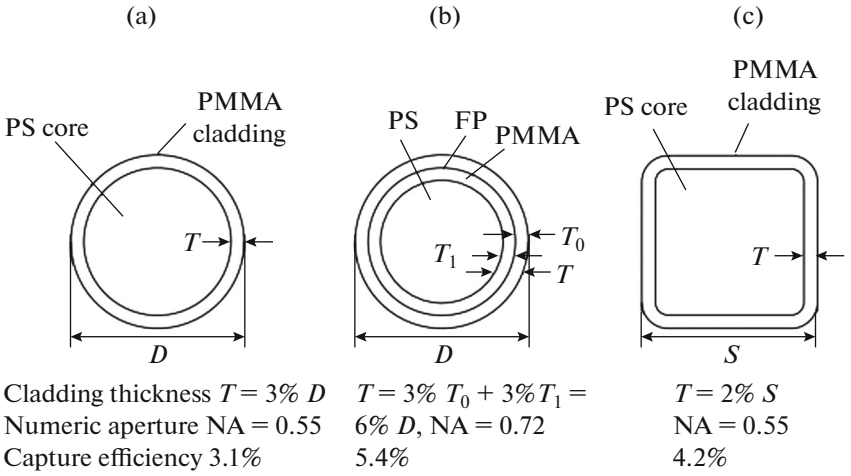

Fig. 27. Structure of fibers: round single-clad (a), round double-clad (b), and square single-clad (c).

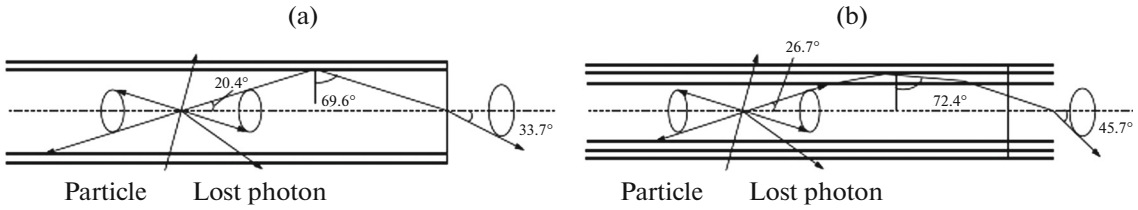

Fig. 28. Diagram of photon propagation in the single-clad (a) and double-clad (b) fibers.

important advantage of SciFi fibers is the minimum occupied space and the minimum material budget.

A multilayered hodoscope was assembled of SCSF-78MJ scintillating fibers 1 mm in diameter at the COMPASS spectrometer for operating in a muon beam at 100–200 GeV/c with the intensity of 10^8 muons/s [43]. The configuration of the fibers in the hodoscope is shown in Fig. 29a. This multilayered hodoscope allowed up to 20 electrons to be collected on a pixel of the multianode H6568 PMT with the temporal resolution of 400 ps. The light yield loss in an 8-mm fiber section irradiated with electrons from the ^{90}Sr source with a dose of 10 kGy (Fig. 29a) was 15%.

It is desirable to place the PD far from the beam region for avoiding a high radiation load on it. To

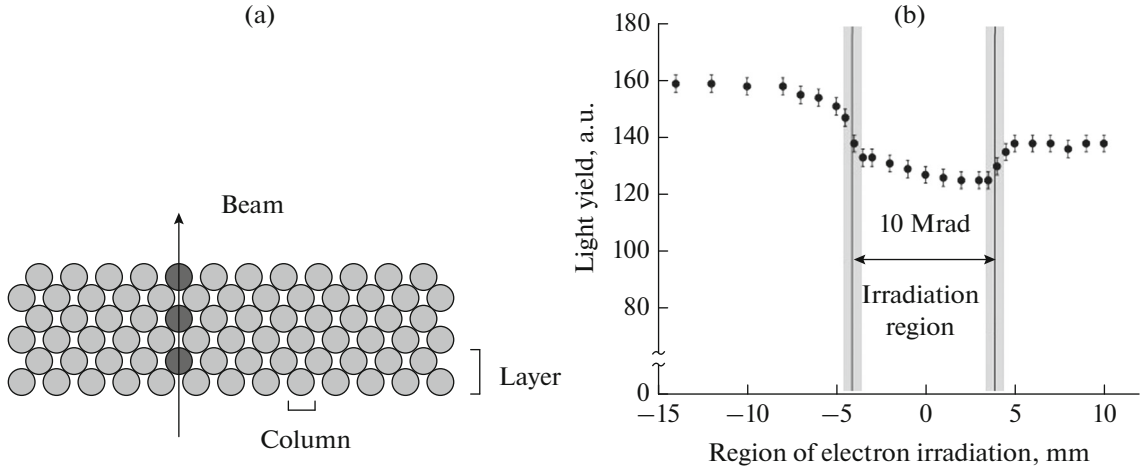

Fig. 29. Arrangement of fibers in a three-layer hodoscope (a) and light yield of Kuraray SCSF-78 fibers irradiated in the indicated region with ^{90}Sr electrons with the dose of 10 kGy (b) [43].

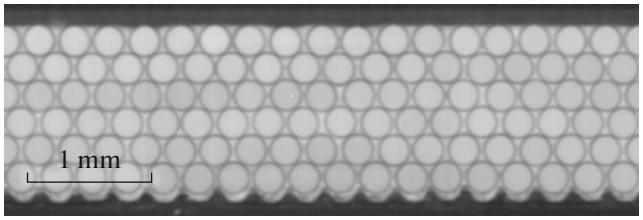

Fig. 30. Cross section of the SciFi fiber detector array [46].

transport light from the SciFi to the PD, the Kuraray PSMJ CF was used, which had a much larger attenuation length than the SciFi.

End-to-end gluing of the scintillating and clear fibers showed that all glues used were adversely affected by radiation and were losing their transparency. Therefore, instead of gluing, the authors used end-to-end welding of the fibers. To this end, the polished faces of the fibers were tightly pressed against each other and kept at a temperature of 105–110°C for a few seconds. The loss of light passing through this contact was <10%.

The attenuation length of CF fibers at the dose of 10 kGy decreased by more than a factor of three. Note that the realistic estimation of the radiation dose shows that in the halo zone it will be an order of magnitude lower than the above-considered one.

In the scope of the LHCb spectrometer upgrade [46, 47] it is planned to replace two tracking systems consisting of gas drift tubes and silicon microstrip detectors with a fiber tracking detector assembled of SCSF-78MJ scintillating fibers 250 μm in diameter. This detector will have two advantages over the existing systems, higher homogeneity and a low material budget (1.1% X_0).

The SciFi fiber detector is assembled of arrays comprising six layers of densely packed 130.65 × 2424.0 × 1.4-mm fibers (Fig. 30). Unlike the traditionally used 3HF, Bicron-12, and SCSF-81 fibers, the SCSF-78MJ fibers had fluors (pTP, tetrabutadiene) in their polystyrene core, which increased the attenuation length and the light yield in comparison to other Kuraray fibers [40]. Signals were read out by a SiPM from one of the fiber ends while the other end was mirrored.

The detector will be subjected to a considerable radiation load, which could amount to 35 kGy for ten years of operation near the beam pipe, rapidly decreasing with distance from the pipe as $\sim 1/r^2$ and reaching 50 Gy at $r = 2.5$ m from the center of the pipe.

Radiation tests of the fibers were carried out at facilities wih different particles that had different energies. The data obtained with proton, γ, and X-ray irradiation with different energies are presented in Fig. 31. According to estimation, the expected light yield loss for the entire detector operation period in the very high radiation areas near the beam will be about 40%.

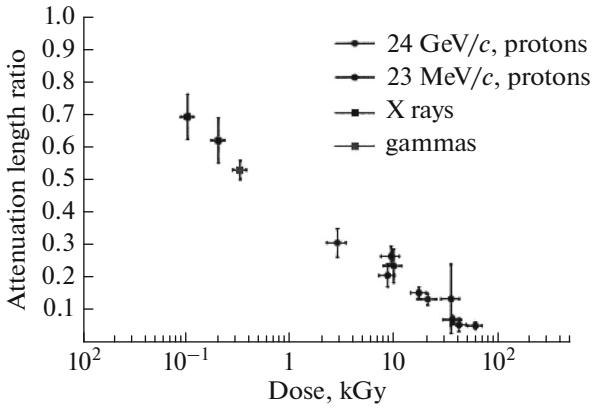

Fig. 31. A compilation of data on the dependence of the attenuation length ratio after and before irradiation of the SCSF-78MJ fiber on the absorbed dose of various particles at various energies [47].

The main cahracteristics of the detector with the 2.4-m-long SCSF-78MJ fibers were measured using pion/proton beams at CERN and electron beams at DESY. The light yield of the fiber array was ~16 photoelectrons, the detection efficiency was 99%, and the spatial resolution was 70 μm [47].

Radiation hardness of Kuraray 3HF S type scintillating fibers 0.5–0.75 mm in diameter with 1% pTP and 1500 ppm 3HF and clear fibers 0.8 mm in diameter was investigated using the ^{60}Co source with low radiation doses of 0.4–500 krad [48]. The S type fibers are characterized by good flexibility due to orientation of their molecules along the fiber. In many experiments CFs are used to transport light from SciFi to a remote PD often through rather hard-accessible areas. In this connection, it was of interest to study radiation hardness of S type 3HF scintillating fibers and clear fibers in relation to the parameter S and the curve radius of the fibers.

Measurements of the dependence of the 3HF SciFi attenuation length on the location of the ultraviolet illumination lamp and the time after irradiation showed a considerable decrease in the attenuation length of the fibers, even at a dose of 10 krad. The attenuation length decreases from 4.5 m (before irradiation) to 2.45 m (13 days after irradiation) (Fig. 32). The irradiation was performed using the ^{60}Co source with the dose of 48 krad at the dose rate of 12 krad/h.

Light yield of the fibers was measured beginning with their length of 45 cm, since at shorter lengths the fibers were protected against radiation. No irregularities are observed in the dose rate dependences of the relative CF and 3HF attenuation lengths after/before irradiation (Fig. 33) in the region of low radiation doses. Extrapolation of the data reduced to the zero length at which the attenuation effect is ruled out shows that fluors are not destroyed at the radiation doses used, as was observed in many studies [19, 30–32].

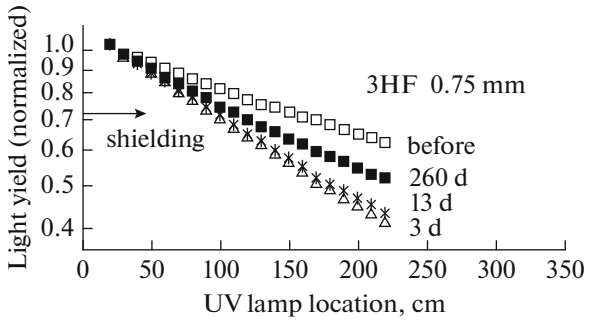

Fig. 32. Dependence of the 3HF fiber light yield, measured before irradiation and 3, 13, and 260 days after irradiation with the dose of 48 krad, on the location of the UV illumination lamp [48].

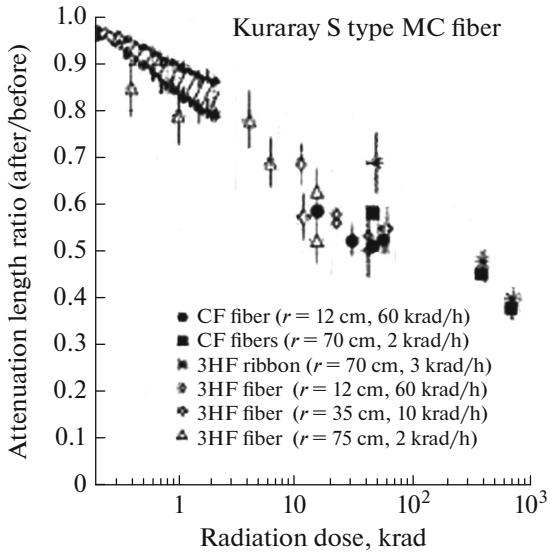

Fig. 33. Attenuation length ratios of the CF and 3HF multiclad (MC) fibers before and after irradiation as a function of the radiation dose at different dose rates and fiber curve radii r [48]. Open symbols are for the 3HF fibers, filled symbols are for the CF fibers, and crosses are for the 3HF fibers arranged in a ribbon.

The ratios between the 3HF and CF attenuation lengths after/before irradiation as a function of the radiation dose show similar behavior (Fig. 33). Measurements were performed 1–2 weeks after irradiation.

The 3HF fibers recover appreciably within several months, and the recovery rate does not strongly depend on the dose rate of 2–12 krad/h and the absorbed dose of 6–48 krad (Fig. 34a).

Dependence of the Kuraray CF attenuation length on the parameter S is shown in Fig. 34b. The attenuation length decreases with increasing parameter S. At $S = 40$ the attenuation length is 12 m, and at $S = 70$ it is 9 m, while the light yield decreases only by 30%. At large S, molecules are more oriented along the fiber axis, and the fiber becomes more flexible, but its transparency deteriorates and the attenuation length decreases (Fig. 34b).

Wavelength-shifting (WLS) fibers. Wavelength-shifting fibers collect light from the scintillator, transform its wavelength, and transport it to the PD. They are widely used in calorimeters and time-of-flight and veto systems. The effect of radiation on light yield and transmittance of WLS fibers depends on their material, absorbed radiation dose, radiation dose rate, and environment.

Fibers can be subjected to irradiation with the same dose either for a short time (high power) or for a long time (low power). The actual result could be different. There are controversial data on the effect of the radiation dose rate on the fiber characteristics and recovery after irradiation. In some studies, this effect was clearly observed [18, 19, 31], and in others it was weakly manifested [16].

The BCF91A-MC, Kuraray Y11(200)MSJ, and S250-100 WLS fibers manufactured by Bicron, Kuraray, and Pol.-Hi.Tech were tested for radiation hardness with the doses of 1.16 and 6.93 kGy from the ^{60}Co source [49]. The fibers were 200 cm long and 1 mm in diameter. Their light yield and attenuation lengths were measured before irradiation and three hours, one day, and six (ten) days after irradiation.

Optical properties of the BCF 91A-MC and Kuraray Y11(200)MSJ fibers before irradiation were almost identical, their attenuation lengths were 280 cm, and light yields differed by no more than 2% (Table 11). The attenuation length Λ_{att} of the Pol.-Hi.Tech S250-100 fiber was 230 cm, its light yield was 81% of the light yield of the other two types of fibers, and the light yield of the BCF 91A-MC fibers had a large spread from fiber to fiber.

The light yields of the fibers irradiated with the doses of 1.16 and 6.93 kGy decreased immediately after irradiation respectively by 13 and 29% (Kuraray),

Table 11. Light yield I of the nonirradiated BCF91A-MC and S250-100 fibers relative to the light yield of the Kuraray Y11(200)MSJ fibers at $x = 140$ cm and the attenuation lengths of these fibers before irradiation [48]

Type of fiber	I ($x = 140$ cm)	RMS, %	Λ_{att}, cm	RMS, %
BC91A MC	0.98	9.6	280	9.5
Y11(200)MSJ	1.00	1.8	280	1.6
S250-100	0.81	5.7	230	5.6

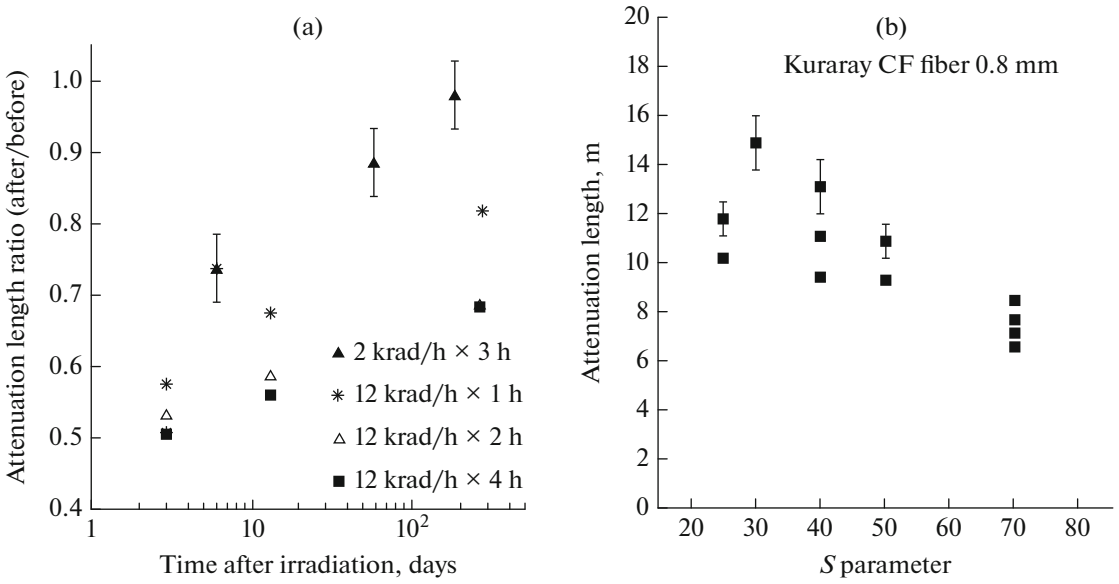

Fig. 34. Dependence of the attenuation length ratio of the 3HF fibers irradiated with different doses at different dose rates on the time after irradiation (a), and dependence of the attenuation length of CF fibers with the diameter of 0.8 mm on the parameter S (b) [48].

17 and 46% (Bicron), and 40 and 48% (Pol.-Hi.Tech) (Table 12). At the dose of 1.16 kGy the decrease in the light yield from the Bicron and Kuraray fibers was almost identical, and at 6.93 kGy the difference in light yield was great. Changes in the Pol.-Hi.Tech S 250-100 yield at both low and high doses were much larger than in Kuraray Y11(200)MSJ (Fig. 35).

With all measurements summarized, it is Kuraray Y11(200)MSJ fibers that show the best light yield and attenuation length both before and after irradiation.

Radiation hardness of the WLS fibers BCF 99-28, BCF 99-28 UVA, and BCF 91A (DC) (Bicron), Y11(200)MS and Y11(200) MS UVA (Kuraray), and S048-100 N4 and S048-100 UVA (Pol.Hi.Tech.) was investigated at low dose rates of ^{60}Co γ-ray radiation and high dose rates of neutron radiation [50]. All fibers had the PS core and the PMMA cladding, and the Kuraray and Bicron fibers had a second cladding of fluorinated PMMA. In addition, all fibers were with and without the ultraviolet absorber (UVA).

The total radiation dose was 140 krad, and the dose rates were 0.55, 1.1, and 4 krad/h. The results were compared with the data obtained at the radiation dose of 1.5 Mrad/h from the mixed beam of the research nuclear reactor, which was comprised of 20% neutrons and 80% γ rays.

The attenuation length Λ_{att} measured three months after the irradiation with 140 krad at the dose rate of 0.55 krad/h was larger in the Kuraray WLS fibers compared to the WLS fibers of the other two manufacturers (Table 13). The light yield of the Bicron and Kuraray fibers did not show dependence on the radiation dose rate irrespective of the presence or absence of the UVA, unlike the S048-100 N4 fibers, in which the UVA effect was observed at a level of 10–15%.

Figure 36 shows light yields of the neutron-irradiated BCF91A, Y11(200)MS, and Y11(200)MS UVA fibers measured 1 h (a) and 1 h to 20 d after irradiation (b). The peak dose of the nuclear-reactor neutrons was 1 Mrad at the dose rate of 1.5 Mrad/h. The primary light yield loss was about 80% for all fibers, and recov-

Table 12. Relative light yield R of the BCF91A-MC, Kuraray Y11(200)MSJ, and S250-100 fibers at $x = 140$ and $x = 30$ cm and at doses of 1.16 and 6.93 kGy

Type of fiber	$\frac{R(140)}{R(30)}$ at 1.16 kGy			$\frac{R(140)}{R(30)}$ at 6.93 kGy		
	0 days	1 day	10 days	0 days	1 day	10 days
BCF91A MC	0.83	0.86	0.85	0.54	0.56	0.56
Y11(200)MSJ	0.87	0.92	0.91	0.71	0.72	0.74
S250-100	0.60	0.70	0.81	0.52	0.55	0.64

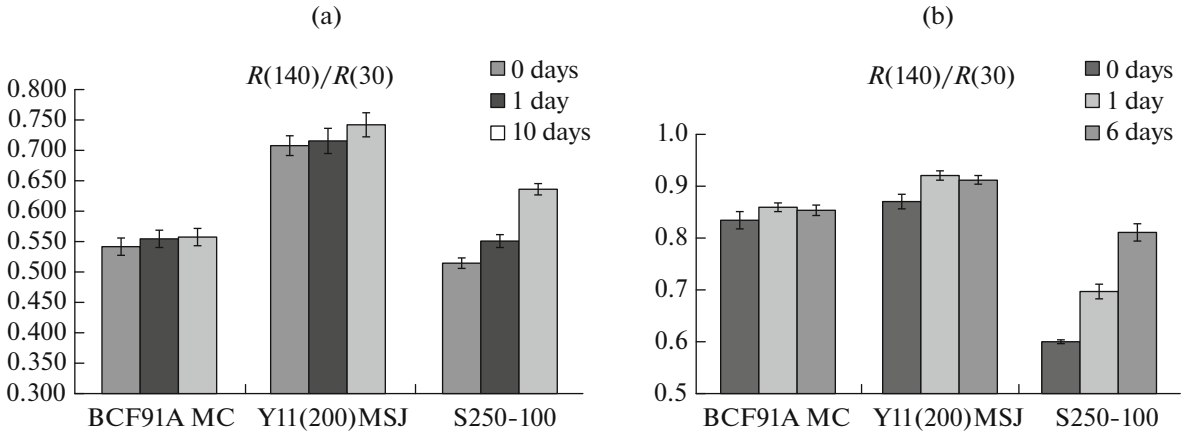

Fig. 35. Light yield ratio $R(140)/R(30)$ of WLS fibers as a function of the recovery time after irradiation with the doses of 6.93 (a) and 1.16 MGy (b).

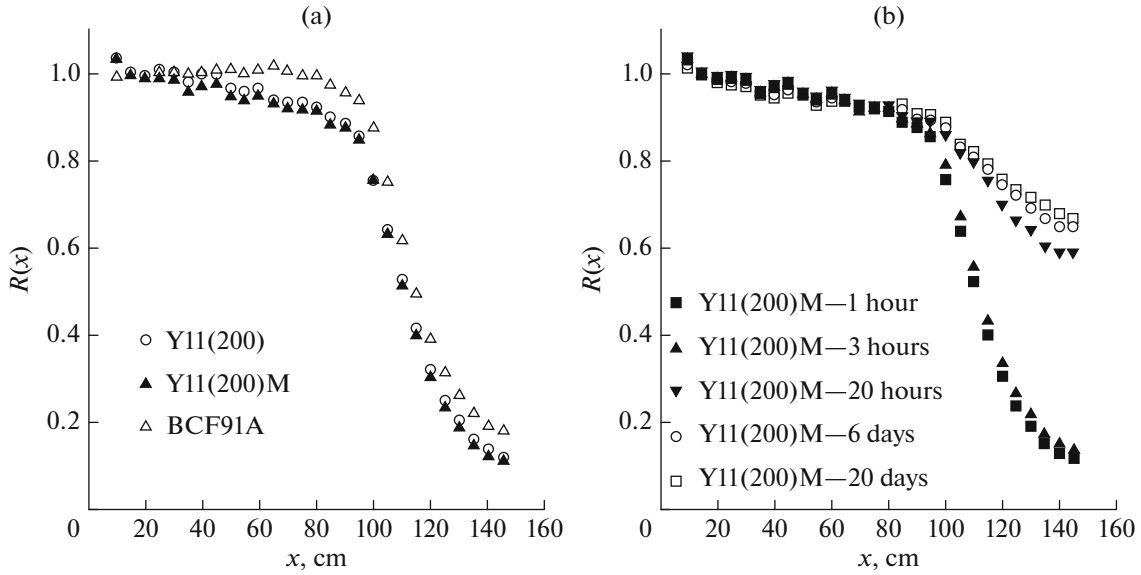

Fig. 36. Light yield ratio $R(x)$ after/before neutron irradiation of the Y11(200), Y11(200)M, and BCF91A fibers 1 h after irradiation (a) and the Y11(200)MS fibers after recovery for different times (b) as a function of the distance to the PD [50].

ery to the residual level took 6–20 days. The residual recovery level was 28% for the Y11(200) and 21 and 24% for the BCF 91A double-clad and single-clad fibers respectively.

In [51], radiation hardness of the BC 9929-MC (Bicron) fiber and the BC-404 scintillator with this fiber were separately studied using the ^{60}Co source. The 30-cm-long fiber was irradiated with doses of

Table 13. The fiber attenuation length (Λ_{att}) before and three months after the irradiation at the dose rate of 0.55 krad/h and absorbed dose of 140 krad

Type of fiber	Λ_{att} (nonirradiated), cm	Λ_{att} (irradiated), cm
BCF99-28 without UVA	260	191
BCF 600 ppмUVA	198	146
BCF91-A	322	201
Y11(200)MS	303	249
Y11 1000 ppмUVA	306	247
S048 100-N4	315	156
S048-100 c UVA	309	189

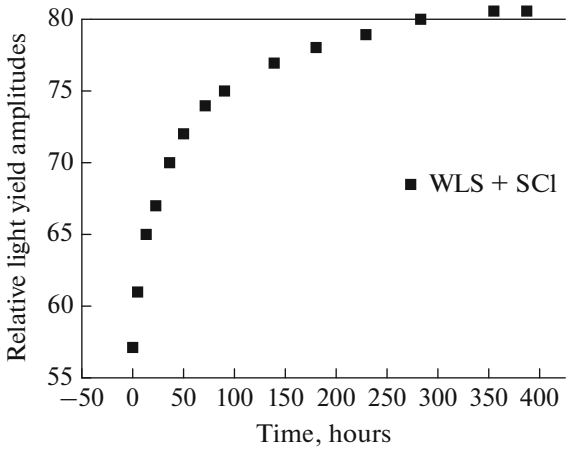

Fig. 37. Relative light-yield amplitude spectra (irradiated/nonirradiated) of scintillators with WLS fibers as a function of time after irradiation [51].

50 krad to 1 Mrad, and the scintillator with the fiber was irradiated with the dose of 200 krad at the dose rate of 4.4 krad/min. The dimensions of the scintillator were 12 × 12 × 1 cm, and the embedded fiber was 25 cm long.

Relative amplitude spectra of the light yield (irradiated/nonirradiated) of the scintillators with the fiber are shown in Fig. 37. The relative change of 80% in the light yield is achieved within 300 hours, which is the time for the sample light yield to reach the constant (residual) recovery level.

The fibers were irradiated with the doses of 50, 100, 200, 300, and 650 krad and 1 Mrad at the dose rate of 7 krad/min. The light yield was measured before and after irradiation with the first four doses (Fig. 38a) and at the higher doses (650 krad, 1 Mrad) (Fig. 38b). Light yield recovery in the fiber was hundreds of times faster than in the scintillator + fiber system (Fig. 38a). At the dose of 1 Mrad the light yield recovered only to 50% of the nonirradiated fiber light yield.

The radiation hardness study of PMMA-based scintillators with the Y7 and K27 fluors and GS218, GS233, and XT 20070 light guides irradiated with the ^{60}Co γ dose of 24 kGy was of interest from the viewpoint of investigating the role of the fluors and the UVA [16]. Absorption spectra of all those materials measured immediately after irradiation behave in a similar way, which indicates that identical absorption centers are produced in them, and their primary damage is associated with the PMMA matrix damage, while possible damage of fluors and UVA is less important (Fig. 39a). Figure 39b shows the wavelength dependence of the recovery of the Y7, GS218, and GS233 light yield to the residual radiation level.

New type of WLS fiber. Scintillating fibers with very short decay time and high light yield based on a new type of fluor (Nanostructured Organosilicon Luminophores, NOLs) are under development at the Institute of Synthetic Polymeric Materials (Moscow) [52, 53].

In an ordinary fiber activators and wavelength shifters are introduced in the core (polystyrene) matrix independently and randomly, and in the new fiber they are connected in polystyrene via silicon atoms, being fixed at a very short (subatomic) distance (Fig. 40). Consequently, energy is transferred from the excited activator molecules to the wavelength shifter via a nonradiative process followed by fast scintillation of the wavelength shifter. Selecting luminophores, one can produce fibers with the given (large) Stokes shifts and excellent temporals characteristics.

Figure 41 shows absorption (a) and emission (b) spectra of the NOL11 and NOL19 luminophores, which were used in the prototypes of the BSF-11-1 and GPF-19-1 scintillating fibers 250 μm in diameter. The NOL11 (NOL19) emission spectrum has the peak in the blue (green) region, and their quantum luminescence efficiency ε and decay time τ are 96% (87%) and 0.98 ns (0.93 ns), respectively (Table 14). For comparison, Fig. 41a also shows the POPOP absorption spectrum. As is seen, the absorption spectrum integral of both luminophores is ~3 times larger than that of POPOP [53].

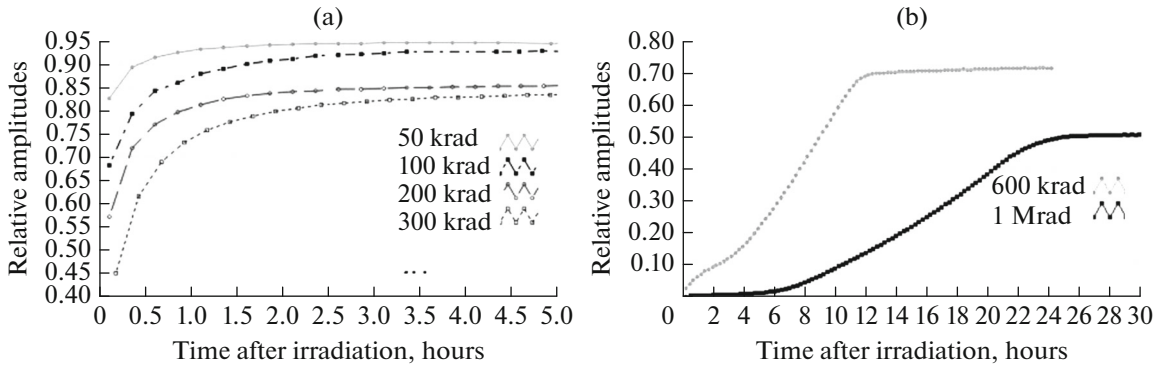

Fig. 38. Relative light yields (irradiated/nonirradiated) of fibers at the radiation doses of 50, 100, 200, and 300 krad (a) and 650 krad and 1 Mrad (b) as a function of time after irradiation [51].

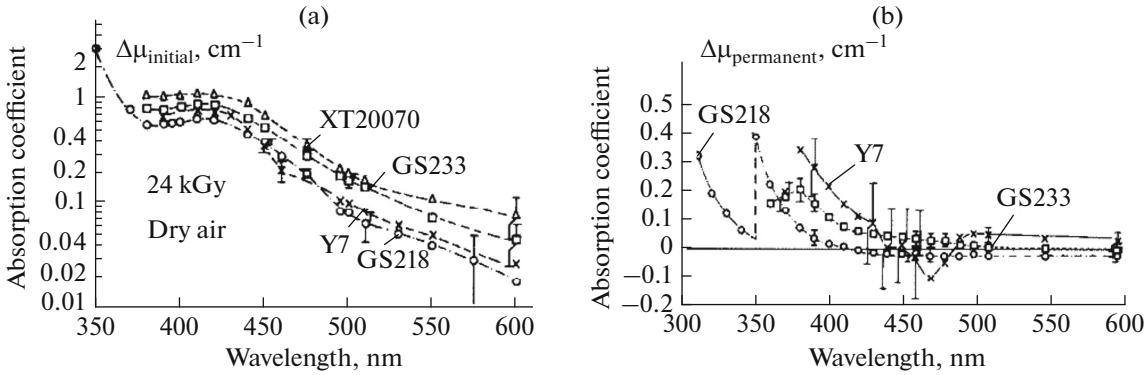

Fig. 39. Absorption spectra of the Y7 WLS fiber (30 ppm) and the GS 218, GS 233, and XT 20070 light guides measured 5–7 days (a) and 1060 days (b) after short-time irradiation in dry air as a function of the wavelength [16].

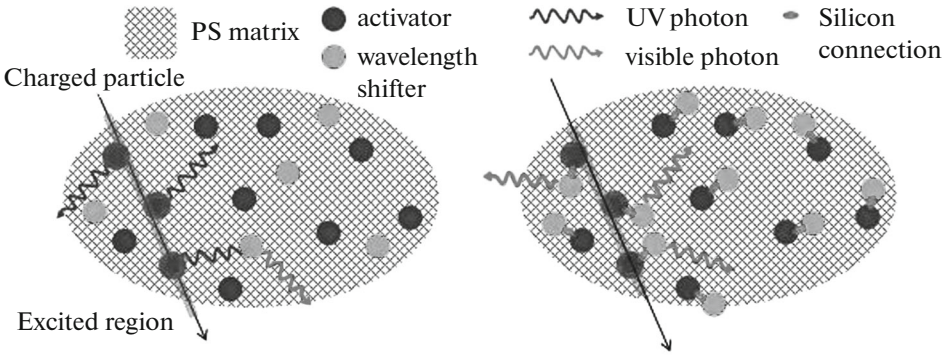

Fig. 40. Diagrammatic view of scintillation light generation in an ordinary PS fiber (a) and a new type of PS fiber with NOL (b) (figure from [46]).

Table 15 presents peak wavelength, measured attenuation lengths Λ_{att}, light yields LY (in photoelectrons), and decay times τ of both prototypes and, for comparison, of most popular blue SCSF-78 and green SCSF-3HF fibers.

The authors consider these data as intermediate. Both prototypes exhibit very short decay times. In the green GPF-19-1 prototype, τ is six times shorter than in SCSF-3HF, and in the blue BPF-11-1 prototype it is almost two times shorter than in SCSF-78.

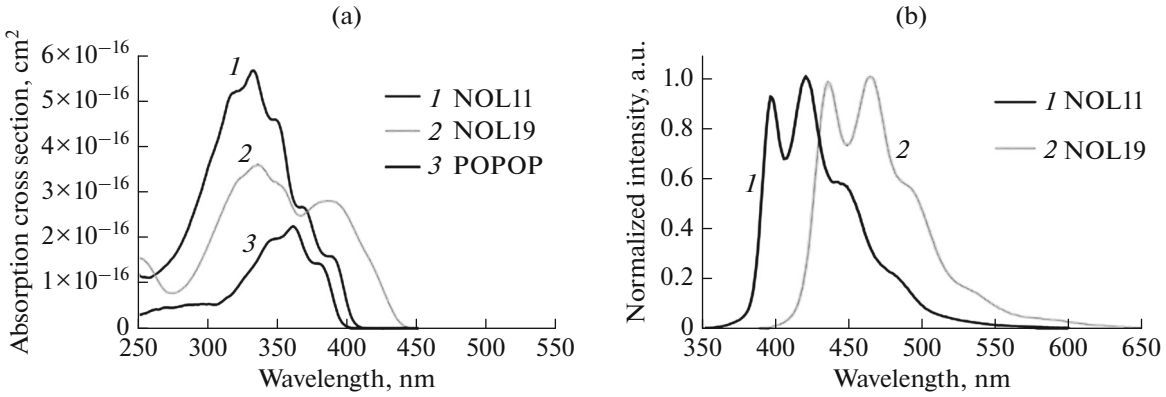

Fig. 41. Absorption spectra of NOL11, NOL19, and POPOP (a) and emission spectra of NOL11 and NOL19 (b) used as efficient wavelength shifters for the BPF-11-1 and GPF-19-1 scintillating fibers [53].

Table 14. Characteristics of the NOL11 and NOL19 luminophores [53]

Luminophore	Λ_{em}, nm	ε, %	τ, ns
NOL 11	391, 421, 445	96	0.98
NOL 19	436, 466, 490	87	0.93

Radiation tests of the BPF-11-1 and GPF-19-1 fibers using X rays with a dose of 1 kGy at the dose rate of 23 Gy/min showed that their radiation hardness is comparable to that of the SCSF-78 and SCSF-3HF fibers. However, X-ray radiation damage can be very different from the damage induced by protons and other particles.

3.3. Optical Glues

Hadronic calorimeters use scintillators in the form of tiles with grooves milled on one of their surfaces for embedding WLS fibers. In neutrino experiments, scintillating strips with grooves or through holes for WLS fibers are used. In all cases, it is extremely important to have maximum efficient light collection.

In past years, light has been collected from scintillators (tiles or strips) by WLS fibers embedded in the grooves on the scintillator surface or inserted in the through holes filled with an optical glue (filler) rather than air alone, which gives considerable gain in light collection. Optical glues must have high transparency and a refractive index close to the refractive index of the scintillator base or the outer cladding of the WLS fiber, which allows reducing loss of light on its passage through the interfaces between the scintillator and the filler (first interface) and between the filler and the outer WLS fiber cladding (second interface).

Table 15. Peak wavelength, attenuation lengths Λ_{att}, light yields $LY_{p.e.}$ (in photoelectrons), and decay times τ of both prototypes and the known SCSF-78 and SCSF-3HF fibers (for comparison) [53]

Fiber	Λ_{peak}, nm	Λ_{att}, cm	$LY_{p.e.}$	τ, ns
BPF-11-1	430	263	23.2	1.34
GPF-19-1	470	294	14.2	1.18
SCSF-78	440	351	27.8	2.36
SCSF-3HF	530	330	23.6	6.18

In the MINOS experiment, the WLS fibers were glued into the grooves on the strip with the BC-600 glue, which led to an increase of up to a factor of 1.8 in light collection [54]. Point gluing of fibers into a strip groove with an optical glue increased light collection up to a factor of 1.6 [55]. Filling of the through hole in the strip with SKTN-MED low-molecular-weight rubber gave a factor of 1.5–1.8 gain in light collection depending on the strip length [56].

Widely used glues are mainly epoxy-based glues EJ-500, Aqua E-30 (MICE–EMR), Araldite Crystal (for MICE–EMR connectors), and BC-600 (for SMRD T2K, MINOS, KLOE). Transmittance of nonirradiated EJ-500, Araldite, BC-600, and Aqua E-30 glues is shown in Fig. 42 [57]. As is seen, it is almost identical for the first three glues in the wavelength range $\lambda > 300$ nm, while for Aqua E-30 it is very different from the others at wavelengths from $\lambda \sim 300$ to $\lambda \sim 400$ nm.

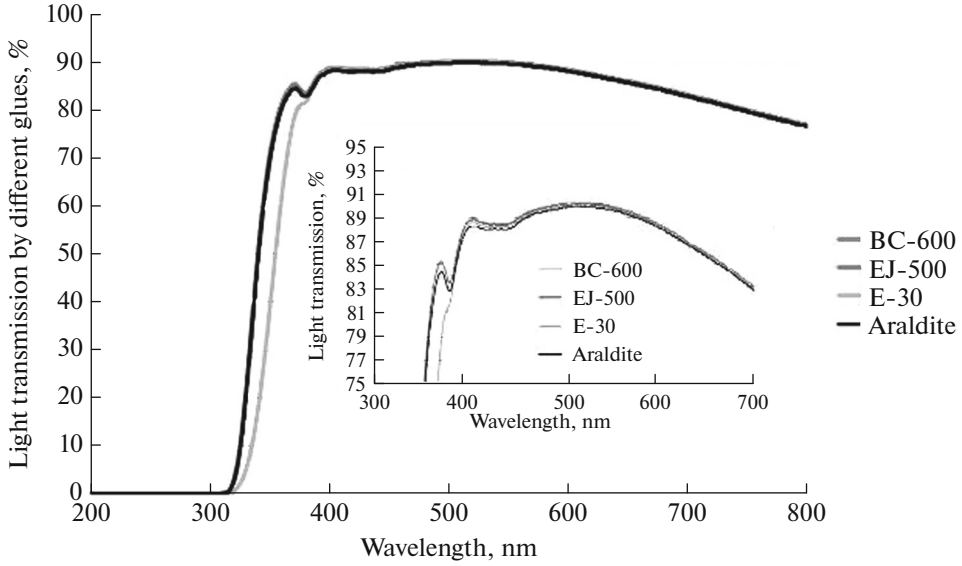

Fig. 42. Light transmission of nonirradiated EJ-500, Aqua E-30, Araldite Crystal, and BC-600 glues as a function of the wavelength [57].

Table 16. Flux densities and fluences of fast neutrons ($E > 1$ MeV) [38]

Position	Flux density, n/cm^2 s	Fluence, n/cm^2	γ background, Mrad
1	1.8×10^9	16×10^{14}	5.4–1.4
2	4.4×10^8	3.8×10^{14}	0.47
3	1.35×10^8	1.2×10^{14}	0.37

It is of great interest to study radiation hardness of popular optical glues. Various fillers in the form of resin (liquid) and glue (polymerized resin) and short polystyrene strip samples with WLS fibers and with and without a filler were irradiated with a neutron beam with $E > 1$ MeV from the JINR IBR-2 fast-pulsed neutron reactor [38]. Flux densities and fluences incident on the samples during their irradiation in three positions are presented in Table 16. The resin and glue layers were about 3 mm thick. The investigated filler was SKTN-MED of grades E and D, which had an identical refractive index of 1.41 at the temperature of 25°C and identical transmittance (over 95%) but different viscosity [58]. Also, for comparison to SKTN-MED, the BC-600 filler with the refractive index of 1.57 and transmittance of >95% widely used in various HEP experiments [59] was irradiated.

Transmittance of the SKTN-MED(D) and BC-600 resins (liquid) and glues (polymerized) irradiated and nonirradiated with neutrons as a function of the wavelength was measured using the SHIMATSU spectrophotometer [60] (Figs. 43, 44). Transmittance of SKTN-MED as a resin (Fig. 43a) and as a glue (Fig. 43b) in the range $\lambda > 400$ nm remains high (>95%) at all neutron fluxes and is only slightly different from transmittance of the nonirradiated samples [61].

Table 17. Long-term stability of light yields and mechanical strength [64]

Scintillator	T_{20} 20% light transmittance	T_{50} 50% mechanical strength
SCSN-81	10	6.2
BC-408	6	5.1
UPS-98RH	8	5.8
UPS-923A	10	8.2

Transmittance of the BC-600 resin (Fig. 44a) and glue (Fig. 44b) turned out to be quite sensitive to neutron irradiation at all neutron fluxes, and the glue was more sensitive to radiation than the resin [61]. Similar behavior of BC-600 was also observed in [62], where BC-600 glue samples 1.5 and 3.0 mm thick were irradiated with Co^{60} γ rays with a dose of 27 kGy (Fig. 45a).

Figure 45b shows the wavelength dependence of the transmittance of the Meltmount samples irradiated with Co^{60} γ rays with a dose of 4 kGy and neutrons and protons with a fluence of 2×10^{13} cm^{-2}. This glue is used in microscopes and, like BC-600, for connecting various optical elements. The refractive index of the Meltmount samples was 1.58, and their thickness was 3 mm [62].

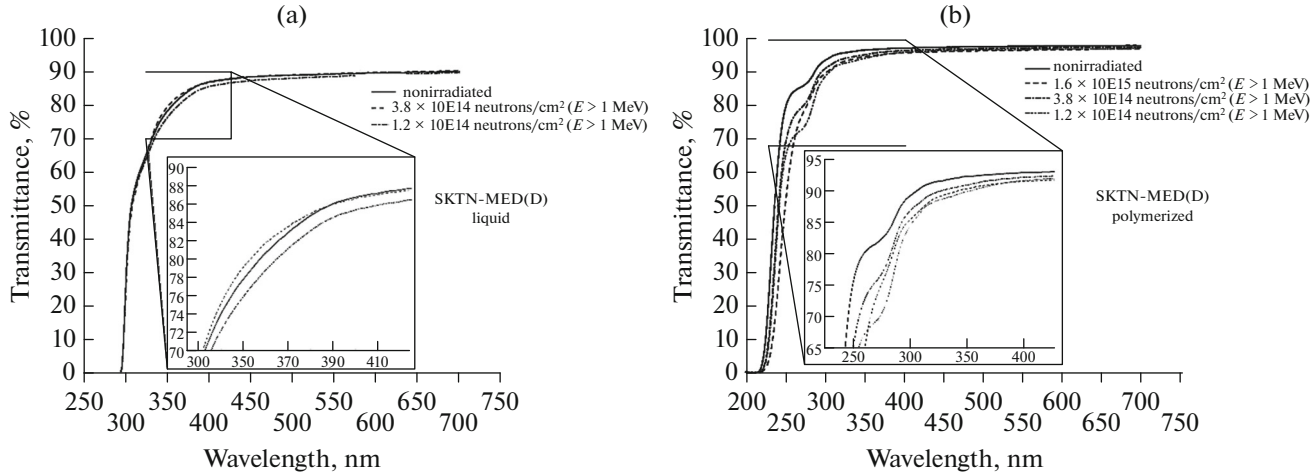

Fig. 43. Transmittance of the SKTN-MED(D) resin (a) and glue (b) as a function of the wavelength before and after irradiation with neutrons with the fluences of 16×10^{14}, 3.8×10^{14}, and 1.2×10^{14} n/cm^2 [61].

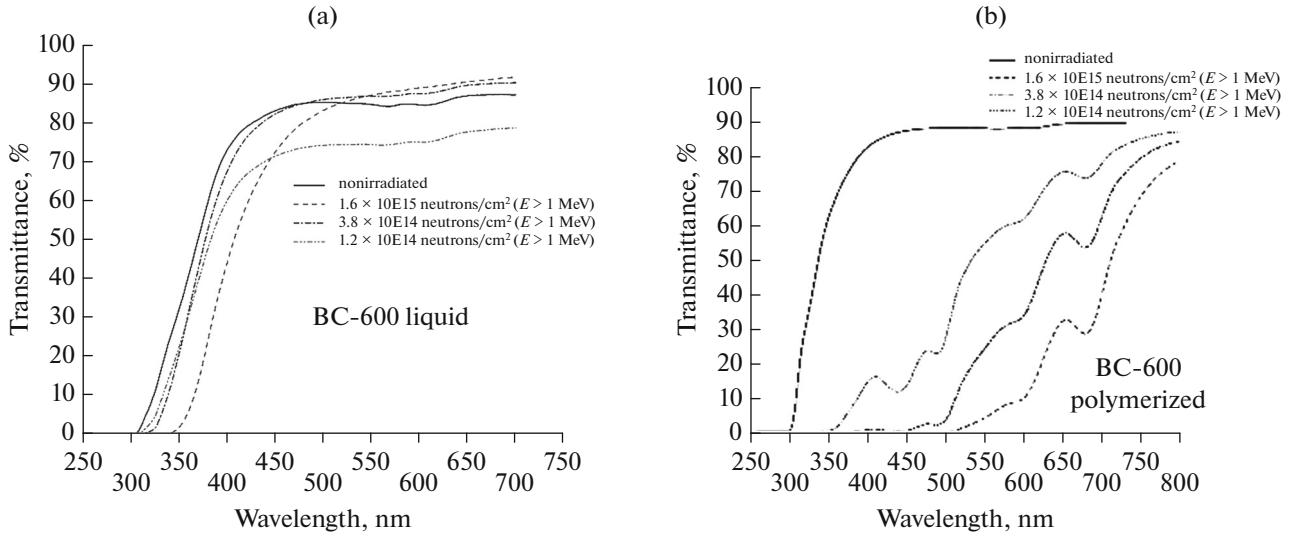

Fig. 44. Transmittance of the BC-600 resin (a) and glue (b) as a function of the wavelength before and after neutron irradiation (16×10^{14}, 3.8×10^{14}, 1.2×10^{14} neutrons/cm^2) [61].

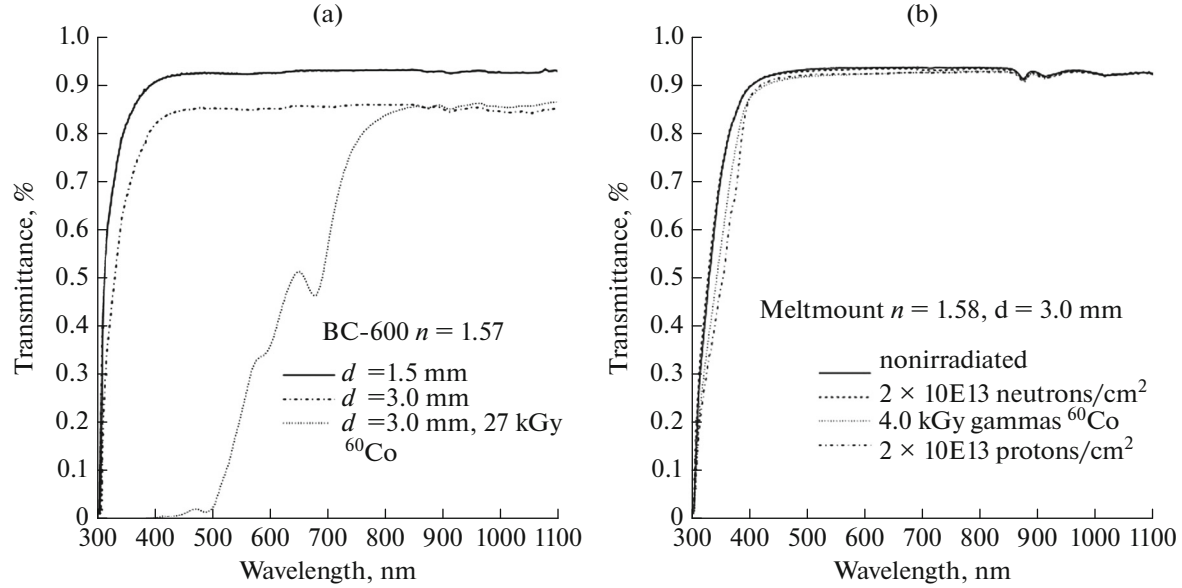

Fig. 45. Transmittance of the BC-600 samples irradiated with ^{60}Co γ rays with the dose of 27 kGy (a) and Meltmount samples irradiated with ^{60}Co γ rays with a dose of 4 kGy and neutrons and protons with a fluence of 2×10^{13} /cm^2 (b) as a function of the wavelength [62].

The effect of radiation on the light yield of short strip samples with a filler and a WLS fiber was studied in [61]. To this end, 15-cm-long strip samples with and without the SKTN-MED(E), SKTN-MED (D), and BC-600 fillers were irradiated with fast neutrons ($E >$ 1 MeV) with fluences of (16, 3.8, 1.2) $\times 10^{14}$ neutrons per 1 cm^2 in beamline 3 of the JINR IBR-2 reactor [38]. Light collection from the "dry" strips and the strips with a filler were measured before and after irradiation by radioactive sources using the Keitley picoammeter [63].

Absolute anode currents of the strips with all three fillers before irradiation were approximately identical, and after irradiation, they were seen to decrease with increasing neutron fluence. For example, the decrease in the anode currents of the irradiated SKTN-MED(D) samples against the currents of the nonirradiated SKTN-MED(D) samples was 85, 67, and 30% at fluences of (16, 3.8, 1.2) $\times 10^{14}$ neutrons/cm^2, respec-

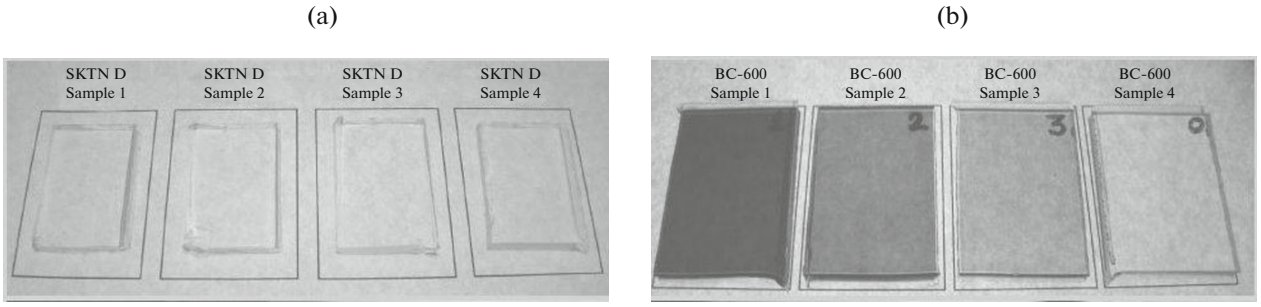

Fig. 46. Photos of plates made of the polymerized resins SKTN-MED(D) (SKTN D) (a) and BC-600 (b), nonirradiated (sample 0) and irradiated with neutrons with the fluences (16, 3.8, 1.2) × 10^{14} cm^2 (plates 1, 2, 3 respectively) [61].

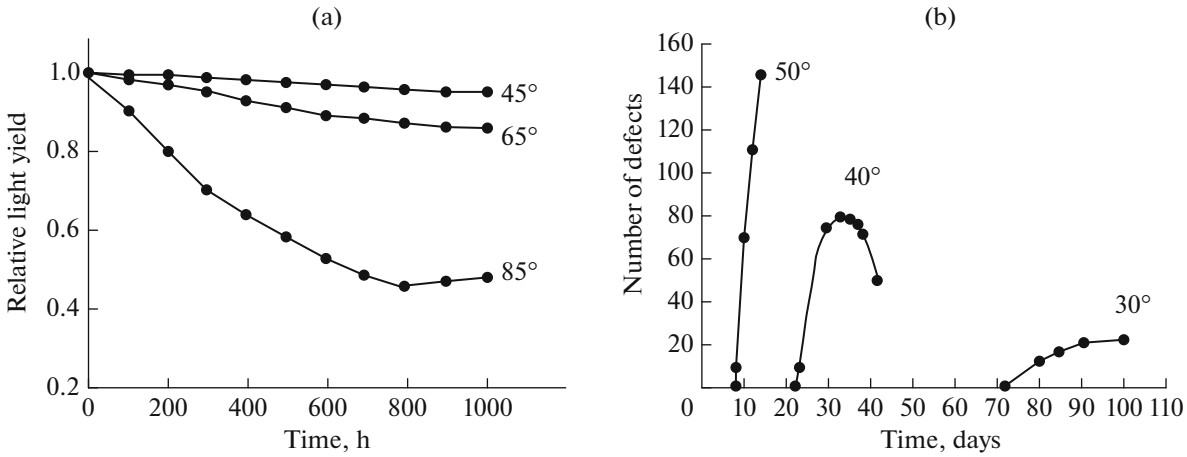

Fig. 47. Exposure time dependence of the variation in the strip light yield at different temperatures (a) and in the number of defects (cracks) in the strip at the humidity of 95% and different temperatures (b) [65].

tively. The corresponding characteristics of SKTN-MED(E) were 85, 46, and 43%. Since transmittance of SKTN-MED at these fluences barely changed, the strip light collection was impaired by the damage of the materials of the strip and the WLS fiber, which affected their light yields.

Figure 46 shows polymerized resin plates of SKTN-MED(D) (designated as SKTN D) (a) and BC-600 (b) irradiated with neutrons with fluences of (16, 3.8, 1.2) × 10^{14} cm^{-2}, numbered 1, 2, and 3 respectively. Plate 0 is a nonirradiated sample. It is well seen that the radiation effect on these fillers is different. Transparency of the SKTN-MED(D) plates hardly changes with the neutron flux (Fig. 46a) while the color of the BC-600 plates changes greatly (Fig. 46b).

4. NATURAL AGING OF SCINTILLATORS

Optical characteristics of scintillators can deteriorate under the effect of not only radiation but also ambient temperature and humidity, which eventually leads to yellowing or even blackening of scintillators and formation of cracks on the surface and in the bulk of the scintillator.

Small samples of the SCSN-81(Kuraray), UPS-98RH and UPS-923A(ISMA, Kharkov, Ukraine) PS-based scintillators, and the BC-408 (Bicron) PVT-based scintillator investigated at normal temperature and humidity showed good long-term stability of their characteristics. Light yield loss of UPS-923A over ten years was no higher than 20%, and mechanical strength loss over 8.2 years was no higher than 50% (Table 17) [64, 65].

However, at temperatures above 65°C ternary PS-based scintillators doped with 2% pTP and 0.02% POPOP suffer appreciable light yield loss (Fig. 47a), and elevated humidity leads to the formation of microcracks, cracking, and yellowing of the scintillator, which results in light collection loss due to light scattering. The number of cracks formed in the scintillator at a humidity of 95% and at three temperatures as a function of the exposure time is shown in Fig. 47b [17].

Aging of BC-92 scintillators was investigated in a wide temperature interval from −30 to 40°C [66]. It was found that in a 2 × 25 × 25-cm scintillator the pre-

Table 18. Effect of heat treatment on radiation hardness of the SCSN-38 scintillator and PMMA-based Y7 and K27 wavelength shifters and GS-218 light guides [69]

Procedure	PMMA-based WLS/light guide	SCSN-38
Heating without irradiation	Only in GS-218: strong additional absorption at 300 nm	No effect at 50°C
Heating before irradiation	Almost no effect	Residual damage level increases with temperature: 15% loss at 70°C, 30% loss at 90°C
Heating after irradiation	All materials recover well in Ar	No effect at 40°C At 88°C residual damage level increases to 70% in 4 days

dictable 20% change in the light yield can occur in 8.7 years, and in a 1 × 25 × 25-cm scintillator with (without) the WLS fiber it occurs in 12.2 (15.3) years.

Aging of the Kuraray SCSF-78M fiber was investigated at temperatures of 40, 55, and 70°C (Fig. 48) [67]. The fiber aging is mainly due to the damage of its core under impact of O_2 in the air. Estimation from the Arrhenius plot shows that at 20°C 10% of light collection can be lost in five years. This lifetime of the fiber can be increased more than twice by decreasing the temperature to 16°C.

Natural aging of Kuraray Y11(200)MSJ WLS fibers was also investigated in [68]. These double-clad fibers with the PS core, inner cladding of PMMA, and outer cladding of fluorinated PMMA were embedded in the grooves of the ATLAS Tile Calorimeter tiles for collecting light signals. The fibers were 1 mm in diameter and 114 to 207 cm long. A half of the fibers had an aluminum coating on one of the ends, and the other half did not.

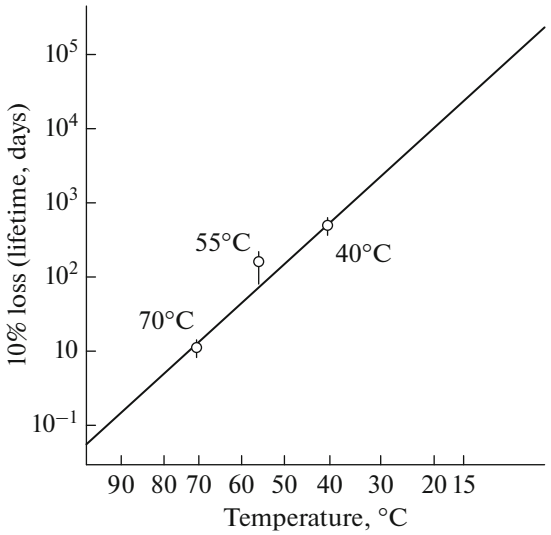

Fig. 48. Lifetime of the Kuraray SCSF-78M (version 1.1 anti-O_2 type) fiber as a function of temperature [67].

Light yield and attenuation length losses of both types of fiber for four years were no larger than 5%. No degradation of the Al coating was observed within experimental errors of 5%.

The effect of heat treatment on the radiation hardness of the SCSN-38 scintillator and PMMA-based Y7 and K27 wavelength shifters and GS-218 and GS-233 light guides with UVA (for absorption of Cherenkov radiation) was studied with irradiated and nonirradiated samples [69].

The PMMA-based samples were irradiated using the ^{60}Co source with a dose of 10 kGy at a dose rate of 0.5 kGy/h and heated to 110°C for 2 h. The SCSN-38 sample was heated to 90°C for 24 h. The results of the transmittance studies are presented in Table 18.

5. CONCLUSIONS

Scintillation detectors based on organic plastic scintillators (OPSs) and optical fibers are basic detectors used in modern accelerator, astrophysics, and neutrino experiments. In connection with the upgrade of the operating accelerators and construction of new ones, long-term stability and reliability of their operation under increasing radiation load attract heightened interest.

Radiation damage (RD) of organic scintillators manifests itself in deterioration of their light yield, transmittance, mechanical and temporal characteristics, and recovery. The amount of RD depends on many factors, such as the radiation dose, dose rate, irradiating particle type, scintillator material, and environment. In past years, the known scintillators and optical fibers have been extensively studied and new materials capable of withstanding elevated radiation load have been searched for.

The experience of using scintillation detectors in the past two or three decades and the results of the recent investigations, though mostly preliminary so far, allow a number of conclusions to be drawn, which can be tentatively divided into two parts, one referring to the results of the "old" studies with radiation doses below 1 MGy (predominantly up to a few of hundreds

of krad) and the other referring to the results of the studies of a few recent years.

Part 1:

(1) RD of organic scintillators and optical fibers increases with decreasing radiation dose rate at identical or similar radiation doses.

(2) RD induced by neutrons with radiation doses of the same order of magnitude, 5.2 and 7.0 kGy, in PS is five times higher than the γ-ray RD, while in PMMA the reverse is true.

(3) RD of organic scintillators and optical fibers are mainly due to destruction in the base matrix rather than in the fluor, though the shape and position of the emission peaks remain unchanged.

(4) Organic aromatic PS and PVT scintillators recover much faster in an O_2 atmosphere than in inert gases, while acrylic PMMA scintillators recover faster in inert gases than in O_2.

(5) Optical fibers recover hundreds of times faster than scintillator + fiber systems at the same radiation doses.

(6) The residual (irrecoverable) level is 5–15%.

(7) Attenuation lengths of optically clear fibers decrease with increasing parameter S (alignment of base molecules along the base axis).

(8) Natural aging of OPSs (at normal temperature and humidity) is slow; it becomes even slower with decreasing temperature and can be longer than 10 years.

Part 2:

(1) Under high radiation loads (>25 MGy) PVT-based scintillators (ELJEN) exhibit higher radiation hardness than PS-based scintillators.

(2) Radiation hardness of scintillators can be increased by increasing concentrations of fluors and using fluors with the emission spectrum shifted to the green region.

(3) Optical fibers based on new luminophores NOL11 and NOL19 have high luminescence efficiency and very short decay times of 1.34 and 1.18 ns.

(4) Scintillators based on polyethylene naphthalate (PEN) exhibit both good radiation hardness and short recovery time, being also very inexpensive.

(5) Time and level of PEN recovery can be considerably improved by exciting the irradiated PEN sample by an RGN LED matrix with the blue emission spectrum.

(6) Segmentation of tiles into strips (finger strips) increases not only their light yield but also their radiation hardness.

(7) Deterioration of the scintillator light yield due to RD can be partially compensated by increasing light collection with the aid of the optical glue, SKTN-MED synthetic low-molecular-weight rubber, inserted between the fiber and the scintillator.

(7) SKTN-MED has not only high optical properties, but also high radiation hardness compared to other known optical glues. Transmittance of SKTN-MED irradiated with neutrons with the fluence of 1.6×10^{15} neutrons/cm^2 in the region of $\lambda > 400$ nm hardly differs from that of nonirradiated SKTN-MED, being above 90%.

ACKNOWLEDGMENTS

The author is grateful to his colleagues J. Budagov, V. Glagolev, Yu. Davydov, A. Artikov, Z. Usubov, D. Chokheli, V. Baranov, I. Vasil'ev, and A. Simonenko for their attention and support of this work.

Detectors and accelerators mentioned in the review:

CERN, the European Organization for Nuclear Research.

LHC, the Large Hadron Collider at CERN with colliding *PP* beams with the cms energy of 14 TeV, luminosity of 2×10^{34} cm^2 s^{-1}, and collision frequency of 40 MHz.

HL-LHC (High Luminosity LHC), the upgraded LHC with the luminosity planned to be 5×10^{34} cm^2 s^{-1} (by 2025).

FCC (Future Circular Collider), a projected accelerator for the energy of 100 TeV supposed to be a successor to the LHC (by 2032).

ATLAS (A Toroidal Large ApparatuS) and CMS (Compact Muon Solenoid), multipurpose spectrometers at the LHC aimed at searching for and investigating Higgs bosons and supersymmetric and other particles.

ALFA, one of the ATLAS detectors intended for high-precision measurement of the LHC luminosity using small-angle proton–proton scattering.

Tile Calorimeter, the ATLAS hadronic calorimeter.

MBTS, the hadron detector in the gap of the Tile Calorimeter.

HE, the CMS endcap hadronic calorimeter.

LHCb (Large Hadron Collider beauty), the single-arm spectrometer at the LHC for investigation of CP asymmetry and rare B-meson decays.

COMPASS (Common Muon and Proton Apparatus for Structure and Spectroscopy), the spectrometer at the SPS for investigation of the nucleon structure and spectroscopy of hadrons in interactions of polarized muon and hadron beams with momentum 160 GeV/*c* with the polarized deuteron target.

FNAL, the Fermi National Accelerator Laboratory (Batavia, United States) housing a proton–antiproton collider (Tevatron) for the cms energy of 1.96 TeV and luminosity of $\sim 3 \times 10^{32}$ cm^{-2} s^{-1}.

D0 and CDF, two main spectrometers at the Tevatron for studying production of heavy quarks and searching for new particles and phenomena. The

Tevatron was shut down in 2011 in connection with the startup of the LHC at CERN.

MINOS (Main Injector Neutrino Oscillation Detector, Fermilab, USA), a detector intended for investigating muon neutrino oscillations.

Mu2e, an experiment at FNAL on the search for very rare processes of conversion of μ mesons to electrons.

JINR, the Joint Institute for Nuclear Research.

NICA **(**Nuclotron-based Heavy Ion Collider fAcility), a heavy-ion collider under construction at JINR.

IBR-2, a fast pulsed neutron reactor at JINR capable of producing neutron fluxes of up to 10^{16} neutrons/cm^2.

FAIR (Facility for Antiproton and Ion Research), an accelerator complex for antiproton and ion investigations under construction in Darmstadt, Germany.

MUSE, a muon–proton scattering experiment at the Paul Scherrer Institute, Switzerland.

T2K (Tokai to Kamioka, Japan), an underground ν detector for the study of ν oscillations.

SMRD T2K, the side muon range detector at the T2K spectrometer.

KLOE (K-Long experiment), a detector at the National Laboratory of Frascati (Italy) for studying CP violation.

REFERENCES

1. J. B. Birks, *The Theory and Practice of Scintillation Counting* (Pergamon Press, London, 1964).
2. R. C. Ruchti, "The use of scintillating fibers for charged particle tracking," Annu. Rev. Nucl. Part. Sci, **46** 281–319 (1996).
3. Yu. N. Kharzheev, "Scintillation counters in modern high-energy physics experiments," Phys. Part. Nucl. **46**, 678–728 (2015), Yu. Kharzheev, "Scintillation detectors in modern high energy physics experiments and prospect of their use in future experiments," J. Lasers, Opt. Photonics, **4** (1), 1000148 (2017).
4. LHC Machine, J. Instrum. **3**, S08001 (2008).
5. F. Zimmermann, in *Proceedings of the First FCC Physics Workshop, CERN, 16–20 January 2017.*
6. www.gsi.de/forschung_beschleuniger/fair.htm
7. V. D. Kekelidze et al. (NICA Collab.), *Design and Construction of Nuclotron-based Ion Collider facility (NICA) Conceptual Design Report* (http://nica.jinr.ru).
8. ATLAS Collab., "The ATLAS experiment at the CERN Large Hadron Collider," J. Instrum. **3**, S08003 (2008).
9. CMS Collab., "The CMS experiment at the CERN Large Hadron Collider," J. Instrum, **3**, S08004 (2008).
10. LHCb Collab., "The Large Hadron Collider beauty experiment at the CERN Large Hadron Collider," J. Instrum. **3**, S08005 (2008).
11. L. Bartoszek et al. (Mu2e Collab.), Mu2e Technical Design Report, FERMILAB-TM-2594, FERMILAB-DESIGN-2014-01, [arXiv:1501.05241].
12. T. Förster, "Zwischenmolekulare energiewanderung und fluoreszenz," Ann. Phys. **437**, 55 (1947).
13. T. O. White, "Scintillating fibers," Nucl. Instrum. Methods Phys. Res., Sect. A **273**, 82 (1988).
14. G. I. Britvich, A. I. Peresypkin, V. I. Rykalin, V. G. Vasil'chenko, L. D. Kornylovskaya, S. A. Malinovskaya, V. T. Skripkina, V. M. Shershukov, E. G. Yushko, A. V. Kulichenko, and A. I. Pyshchev, "Radiation damage studies on polystyrene-based scintillators," Nucl. Instrum. Methods Phys. Res., Sect. A **326**, 483–488 (1993).
15. R. J. Woods and A. K. Pikaev, *Applied Radiation chemistry: Radiation processing* (J. Wiley, New York, 1994).
16. K. Wick, D. Paul, P. Schröder, V. Stieber, and B. Bicken, "Recovery and dose rate dependence of radiation damage in scintillators, wavelength shifters and light guiders," Nucl. Instrum. Methods Phys. Res., Sect. B **61**, 472–486 (1991).
17. V. G. Senchishin, F. Markley, V. N. Lebedev, and V. E. Kovtun, V. S. Koba, A. V. Kuznichenko, V. D. Tizkaja, J. A. Budagov, G. Bellettini, V. P. Sehnozbenkova, I. I. Zalubovsky, and I. E. Chirikov-Zorin, "A new radiation stable plastic scintillator," Nucl. Instrum. Methods Phys. Res., Sect. A **360**, 253–257 (1995).
18. A. D. Bross and A. Pla-Dalmau, "Radiation effects in intrinsic 3HF scintillator," Nucl. Instrum. Methods Phys. Res., Sect. A **327**, 337– 345 (1993); A. D. Bross and A. Pia-Daimau, IEEE Trans. Nucl. Sci. **NS-39**, 1199 (1992).
19. C. Zorn, M. Bowen, S. Majewski, J. Walker, and R. Wojcik, "A new polyvinyltoluene-based, radiation-resistant plastic scintillator," Nucl. Instrum. Methods Phys. Res., Sect. A **271**, 701–703 (1998); C. A. Zorn, "Pedestrian guide to radiation damage in plastic scintillators," Nucl. Phys. (Proc. Suppl.) **32**, 377–383 (1993).
20. N. Emanuel and A. Buchachenko, *Chemical Physics of Polymer Degradation and Stabilization*, (VNU Science Press, 1987).
21. S. Liao et al., "A comparative study of the radiation hardness of plastic scintillators for the upgrade of the Tile Calorimeter of the ATLAS detector," J. Phys.: Conf. Ser., **645**, 012021 (2015); Jivan H. et al. "Radiation damage effects on the optical propertieis of plastic scintillators," Nucl. Instrum. Methods Phys. Res. Sect. **B 409**, 224–228 (2017).
22. V. Rykalin, V. Brekhovskikh, S. Chernichenko, A. Gorin, and V. Semenov, "Development of polystyrene scintillator technology and particle detectors on their base," J. Phys. Sci. Appl. **5**, 6–13 (2015).
23. ISMA (Institute for Scintillation Materials), Kharkov, Ukraine, www.isma.kharkov.ua/eng/
24. Bicron Corp., 12345 Kisman Rd. Newbury ON 440 USA.
25. CMS HCAL Collab., "Brightness and uniformity measurements of plastic scintillator tiles at the CERN H2 test beam," J. Instrum. **13**, 01002–10004 (2018).
26. www.eljentechnology.com/

27. E. Tiras, J. Wetzel, B. Bilki, D. Winn, and Y. Onel, "Development of radiation hard scintillators," arXiv:1611.05228v1 [physics.ins-det]. Cited November 16, 2016.
28. Scintirex Brand Scintillator, http://www.teijin.com/news/2011/ ebd110907_00.html. Cited November 2, 2016.
29. J. Wetzel et al., "Using LEDs to simulate the recovery of radiation damage to plastic scintillators," Nucl. Instrum. Methods Phys. Res., Sect. B **395**, 13–16 (2017).
30. Zhao Li et al., "Properties of plastic scintillators after irradiation," Nucl. Instrum. Methods Phys. Res., Sect. A **552**, 449–455 (2005).
31. E. Biagtan et al., "Effect of gamma radiation dose rate on the light output of commercial polymer scintillators," Nucl. Instrum. Methods Phys. Res., Sect. B **93**, 296–301 (1994).
32. V. Khachatryan et al., "Dose rate effects in the radiation damage of the plastic scintillators of the CMS Hadron Endcup Calorimeter," J. Instrum. **11**, T10004 (2016).
33. P. C. Trimmer, J. B. Schlenoff, and K. F. Johnson, "Spatially resolved uv-vis characterization of radiation-induced color centers in poly(styrene) and poly(vinyltoluene)," Radiat. Phys. Chem. **41**, 57 (1993).
34. M. Hamada et al., "Radiation damage studies on the optical and mechanical properties of plastic scintillators," Nucl. Instrum. Methods Phys. Res., Sect. A **442**, 148–154 (1999).
35. B. Bodmann and U. Holm, "Neutron-irradiated plastic scintillators," Nucl. Instrum. Methods Phys. Res., Sect. B **185**, 299–304 (2000).
36. S. V. Afanasiev, P. de Barbaro, I. A. Golutvin, I. F. Emeliantchik, A. I. Malakhov, P. V. Moisenz, V. A. Smirnov, and N. M. Shumeiko, "Improvement of radiation hardness of the sampling calorimeters based on plastic scintillators," Nucl. Instrum. Methods Phys. Res., Sect. A **717**, 11–13 (2013).
37. S. V. Afanasiev et al., "Light yield measurements of "finger" structured and unstructured scintillators after gamma and neutron irradiation," Nucl. Instrum. Methods Phys. Res., Sect. A **818**, 26–31 (2016).
38. M. Bulavin, A. Cheplakov, V. Kukhtin, E. Kulagin, S. Kulikov, E. A. Shabalin, and A. Verkhoglyadov, "Irradiation facility at the IBR-2 reactor for investigation of material radiation hardness," Nucl. Instrum. Methods Phys. Res., Sect. B **343**, 26–29 (2015).
39. J. E. Mdhluli et al., "High fluence neutron radiation of plastic scintillators for the TileCal of the ATLAS Detector," High Energy Particle Physics Workshop (2017), IOP Conf. Series, J. Phys.: Conf. Ser. **889**, 012009 (2017).
40. Kuraray Corp., Japan, Wavelength Shifting Fibers, http://kuraraypsf.jp/psf/ws.html.
41. Bicron Corp., U.S.A., Scintillating Fibers. www.crystals.saint-gobain.com/Scintillating_Fiber.aspx.
42. S. Ask et al. (ATLAS Collab.), "Luminosity measurement at ATLAS—development, construction and test of scintillating fibre prototype detectors," Nucl. Instrum. Methods Phys. Res., Sect. A **568**, 588–600 (2006).
43. J. Bislinghoff et al., "A scintillating fibre hodoscope for high rate applications," Nucl. Instrum. Methods Phys. Res., Sect. A **490**, 101–111 (2002).
44. E. O. Cohen, E. Piasetzky, Y. Shamai, and N. Pilip. "Development of a scintillating-fiber beam detector for the MUSE experiment," Nucl. Instrum. Methods Phys. Res., Sect. A **815**, 75–82 (2016).
45. V. M. Abazov et al. (D0 Collab.), "Upgraded D0 Detector," Nucl. Instrum. Methods Phys. Res., Sect. A **565**, 463–532 (2006).
46. C. Joram, G. Haefeli, and B. Leverington, "Scintillating fibre tracking at high luminosity colliders," J. Instrum. **10**, CO8005 (2015).
47. P. Hopchev, SciFi: A large scintillating fibre tracker for LHCb, arXiv:1710.08325v1 [physics.ins-det]. Cited October 23, 2017.
48. K. Hara, K. Hata, S. Kim, M. Mishina, M. Sano, Y. Seiya, K. Takikawa, M. Tanaka, and K. Yasuoka, "Radiation hardness and mechanical durability of Kuraray optical fibers," Nucl. Instrum. Methods Phys. Res., Sect. A **411**, 31–40 (1998).
49. M. J. Varanda, M. David, A. Gomes, and A. Maio, "Recent results of radiation hardness tests of WLS fibers for the ATLAS TileCal hadronic calorimeters," Nucl. Instrum. Methods Phys. Res., Sect. A **453**, 255–258 (2000).
50. A. Maio, M. David, and A. Gomes, "Dose rate effects in WLS fibers," Nucl. Phys. (Proc. Suppl.) **54**, 222–228 (1997).
51. R. Alfaro, E. Cruz, M. I. Martinez, L. M. Montaño, G. Paic, and A. Sandoval, "Radiation hardness tests of a scintillation detector with wavelength shifting fiber readout," in *Particles and Fields: X Mexican Workshop on Particles and Fields, Part A* (AIP, 2006),
52. S. A. Ponomarenko et al., "Nanostructured organosilicon luminophores and their application in highly efficient plastic scintillators," Sci. Rep. **4**, 6549 (2014).
53. O. Borshchev, A. B. R. Cavalcante, L. Gavardi, L. C. Gruber, C. Joram, S. Ponomarenko, O. Shinji, and N. Surin, "Development of a new class of scintillating fibres with very short decay time and high light yield," J. Instrum. **12**, 05013 (2017).
54. D. G. Michael, J. Trevor, A. Sousa, D. Jensen, and B. R. Becker, et al. "The magnetized steel and scintillator calorimeters of the MINOS experiment," Nucl. Instrum. Methods Phys. Res., Sect. A **596**, 190–228 (2008).
55. G. I. Britvich, V. V. Brekhovskikh, V. K. Semenov, and S. S. Kholodenko, "The main characteristics of polystyrene scintillators produced at the Institute of High-Energy Physics and detectors of their basis," Instrum. Exp. Tech. **58**, 211–230 (2015).
56. A. Artikov, V. Baranov, Yu. Budagov, D. Chokheli, Yu. Davydov, V. Glagolev, Yu. Kharzheev, et al. "Optimization of the light yield by injecting an optical filler into the co-extruded hole of the plastic scintillation bar," J. Instrum. **11**, T05003 (2016).
57. E. Noak and T. Schneider, "AIDA optical glue transmission tests," http://cds.cern.ch/AIDA-rep-2015-001.
58. Research and production enterprise SYREL, Russia, SKTN-MED low molecular-weight rubber. http://www.surel.ru/silicone/77/.

59. Bicron Corp., USA, BC-600, Optical Cement. www.crystals.saintgobain.com/.../sgc-bc600-data-sheet_69724.pdf.
60. Spectrophotometer, SolidSpec-3700 DUV SHIMATSU, Japan.
61. A. Artikov, V. Baranov, Yu. Budagov, M. Bulavin, D. Chokheli, Yu. I. Davydov, V. Glagolev, Yu. Kharzheev, V. Kolomoets, A. Simonenko, Z. Usubov, and I. Vasiljev, "Light yield and radiation hardness studies of scintillator strips with a filler," arXiv:1711.11393v1 [physics.ins-det]. Cited 30 Nov 2017.
62. Th. Kirn, M. Haring, D. Schmitz, and W. Schulz, "Absorption length, radiation hardness and ageing of different optical glues," CMS-NOTE-1999-003; http://cms.cern.ch/record/68707 (08/23/2018).
63. Keitley Products, TEKTRONIX INC, US, Keitley6487, picoammeter; http://w.tek.com/sites/tek.com/files/media/resources/6487.pdf (08.23.2018).
64. V. D. Grinev and V. G. Senchishin, *Plastic Scintillators* (Akta, Kharkov, 2003) [in Russian].
65. A. Artikov, J. Budagov, I. Chirikov-Zorin, D. Chokheli, M. Lyablin, G. Bellettini, A. Menzione, S. Tokar, N. Giokaris, and A. Manousakis-Katsikakis, "Properties of the Ukraine polystyrene-based plastic scintillator UPS 923A," Nucl. Instrum. Methods Phys. Res., Sect. A **555**, 125–131 (2005).
66. Zhou Tianfu, He Huihai, and Sheng Xiangdong, "The long-term stability of plastic scintillator for electromagnetic particle detectors," in *Proceedings of the 32nd International Cosmic Ray Conference, August 11–18, 2011, Beijing, China*.
67. A. Susuki et al., "Design, construction, and operation of SciFi tracking detector for K2K experiment," Nucl. Instrum. Methods Phys. Res., Sect. A **453**, 165–176 (2000).
68. J. Silva, A. Maio, J. Pina, J. Santos, and J. G. Saraiva, "Ageing studies of wavelength shifter fibers for the TILECAL/ATLAS experiment," Nucl. Instrum. Methods Phys. Res., Sect. A **580**, 318–321 (2007).
69. B. Bicken, A. Dannemann, U. Holm, T. Neumann, and K. Wick, "Influence of temperature treatment on radiation stability of plastic scintillator and wave-length shifter," IEEE Trans. Nucl. Sci. **39**, 1212–1216 (1992).

Translated by M. Potapov